INTRA-OCEANIC SUBDUCTION INITIATION BASED ON ANALOGUE MODELLING

Michail Delagas

Utrecht University

Earth Structure and Dynamics

Department of Earth Sciences

University of Utrecht

This dissertation is submitted for the degree of Master in Sciences

July 2019

Acknowledgments

During the writing of this Master Thesis I have never been alone and I always been supported and assisted. For this reason I want to acknowledge the important role of my supervisors Dr. Ernst Willingshofer and PhD student Antoine Auzemery for their help on the formulation of this research topic and for their contribution with their expertise not only by helping me develop the required experimental techniques but also for the knowledge I obtained from their fruitful and inspiring scientific conversations during all the past academic year.

In addition, I would like to mention the very important to me, help and immediate response on any issues or questions I had during the experimental procedure from Dr. Dimitrios Sokoutis and the laboratory assistant and Master student Job Arts.

Last but not least I would like to express my gratitude to my family who they were always there supporting me with any means they had, and also to my girlfriend and best friend Nicolette who always had a sympathetic ear for me and was patient with my inconvenient and tight schedules especially of the past few months.

CONTENTS

Abstract

Subduction is key for driving for plate tectonics. Yet it is still unclear where and how subduction initiates in the oceanic domain. It is widely accepted that it critically depends on the rheology of the oceanic lithosphere (Nikolaeva et al., 2010) and can occur upon failure of the load-bearing crustal and mantle layers. When oceanic lithosphere is too strong, high shear strength of the oceanic lithosphere does not permit failure, and subduction may occur by deforming a passive margin at ocean-continent transition. However, weakening processes such as zones of serpentinized mantle may affect the strain localization (*Maffione et al., 2015; Stern 2004)*. Therefore, a series of experiments conducted to determine the favourable rheological and kinematic conditions that lead to the development of subduction zones in the intra-oceanic domain. These experiments involving both oceanic and continental domains which incorporate weak zones of realistic dimensions in the oceanic crust. Model results show that the key factor for the strain localisation is the difference in strength between the continental and oceanic upper crust. Analysis of deformation is used to define a boundary of rheological conditions enabling subduction in oceanic or in continental domain. Additionally, addition of a weak zones in a thick and strong oceanic lithosphere doesn't affect the deformation pattern. However, presence of a weak zone in a relatively younger oceanic lithosphere (60 ± 10 My) may induce strain localization in the oceanic crust rather than at passive margin. This shows the importance of geological inheritance and thermo-mechanical feedbacks for the locus and evolution of subduction zone.

1 INTRODUCTION

Subduction is one of the most important and crucial processes for the renewal of earth's crust and the viability of the tectonic cycle. It is generally accepted that spontaneous initiation of this process most likely occurs where weakened zones of the crust are existing such as transformation/fracture zones. Principally, the subduction of a lithospheric plate starts when the lithosphere becomes denser than the underlying asthenospheric mantle and consequentially is able to sink (Robert J. Stern, 2004). However, at passive margins, several studies on subduction initiation (SI) suggest that the stresses are not large enough to overcome the flexural resistance of an oceanic lithosphere (McKenzie, 1977);(Mueller & Phillips, 1991; Cloetingh, Wortel, & Vlaar, 1982). Gradually, tectonic scenarios have been discussed by geologists to explain the significance of weak zones for the nucleation of subduction, without however focusing on the balance of forces and locations of these weaknesses (Robert J Stern & Gerya, 2018). Observations from natural cases on the other hand, suggest that subduction may occur at the Ocean-Continent Boundary (OCB) (Casey & Dewey, 1984; Dewey & Bird, 1970; Karig, 1982). Several researches have been done and theories have been developed over the years to address this problem. Analogue and numerical modelling studies support the idea that SI occurs in three stages: (1) failure of the brittle crust, (2) over-thrusting of the continental lithosphere, and (3) the subduction stage proper involving the sinking of the oceanic lithosphere into the asthenospheric mantle (Goren et al., 2008; K. Nikolaeva, Gerya, Gerya, Marques, & Marques, 2010). Failure of the crust at the OCB is favored by the fact that the thinning of the continental crust weakens the continental margin as it has been observed in natural passive margins (PM) (Yamato, Husson, Becker, & Pedoja, 2013). Therefore, crustal failure creates lithosphere deflection inducing under-thrusting of the oceanic lithosphere. At this stage, subduction is mainly controlled by the ductile strength of the lithospheric mantle. It follows that either lateral strength difference between rheological layers play a key role in SI (K. Nikolaeva et al., 2010; Calignano et al., 2017), or that the strength of the mantle lithosphere drives the under-thrusting stage, and that subduction can occur mainly for a young margin with a relatively weak lithospheric mantle, e.g. for a time range of 20 to 70 Myr after rifting (England and Wortel, 1980). Moreover, lateral rheological and structural heterogeneities such as oceanic detachment faults (e.g. Cann et al., 1997, Escartin et al., 2003, Smith et al., 2008) in the oceanic crust and may be enough to trigger under-thrusting (Stern and Gerya 2018 and references there). What would be the favorable parameter combination in terms of oceanic lithosphere thickness, strain rate and rheological heterogeneities for subduction initiation in the oceanic domain? Is a weakness in the oceanic crust enough to localize deformation and initiate subduction even if the oceanic plate is thin and not buoyant enough? Therefore, this study proposes to define favorable parameter combination for subduction initiation in the oceanic domain. To address this question, intra-

oceanic subduction initiation will be simulated by analogue modeling through a series of experiments where oceanic and continental lithospheres are submitted to compression. The gradually growing complexity of the oceanic lithosphere setting (in terms of strain rate, thickness, heterogeneity etc.) will lead to the conclusion whether or not a young and buoyant oceanic crust is able to sink and subduct under a lithosphere with oceanic origin under compression.

1.1 Intra-oceanic subduction

40% of the subduction zones on the Earth are intra-oceanic (e.g. Marianna, Aleutian or Lesser Antilles subduction zones) (Figure 1.1) yet it is not clear how they came into existence, because the rheological conditions initiating the rupture and failure of an oceanic lithosphere are particularly poorly constrained. It is believed that gravitational instabilities play a key role in this natural process (Vlaar & Wortel, 1976). The density of an oceanic lithosphere becomes greater than the underlying asthenosphere's within 10-50 Myr following its formation. Plate rupture and subsequent subduction of the oceanic plate, however, remains difficult as oceanic lithosphere is too stiff to become convectively unstable, preventing lithospheric bending and failure (Solomatov, 1995). Thus, a young and weaker oceanic lithosphere doesn't have the required density to sink spontaneously in the asthenosphere while an old and dense lithosphere is too strong to break. It can be concluded that intra-oceanic subduction initiation requires a lithosphere weak enough to overcome the flexural resistance and break, and at the same time being dense enough to be able to sink and form a slab. So, even if the oceanic lithosphere is homogenous and compression occurs, force transfer will favor subduction

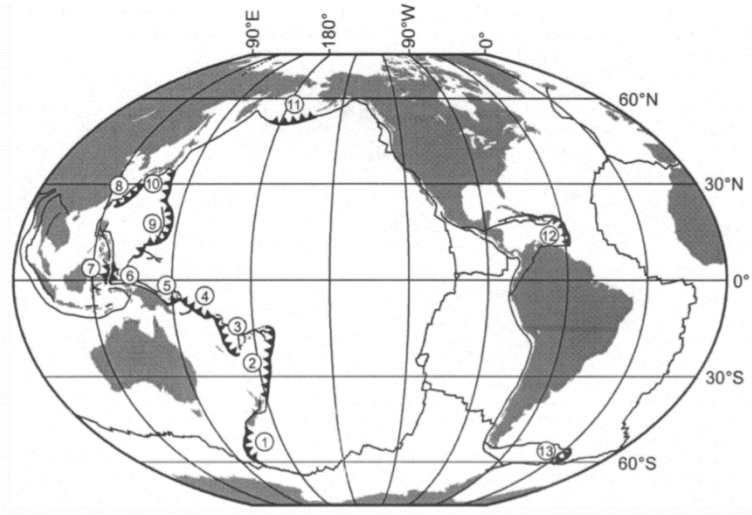

Figure 1.1 Active intra-oceanic subduction zones (Leat and Larter 2003). Thick lines show the intra-oceanic subduction zones and thin lines represent the rest of plate margins. The numbers in the circles indicate the names of the following active intra-oceanic subduction systems: 1, MacQuarie; 2, Tonga-Kermadec; 3, Vanuatu (New Hebrides); 4, Solomon; 5, New Britain; 6, Halmahera; 7, Sangihe; 8, Ryukyu; 9, Mariana; 10, Izu-Ogasawara (Bonin); 11, Aleutian; 12, Lesser Antilles; 13, South Sandwich.

initiation at ocean-continent transition (OCT) where lateral strength differences are large (Auzemery et al. 2019, in revision). Inherited structures and features of the crust related to past weakening processes such as serpentinisation, appear to play an important role on the deformation of passive margins (Toth and Gurnis, 1998; Hall et al., 2003; Gurnis et al., 2004).

It is thus suggested that weak zones in oceanic domain strongly controls intra-oceanic subduction initiation. In this sense, two hypotheses were largely debated:

1. Mainly based on geological evidence coming from ophiolitic belts, 2-d numerical models (Maffione et al., 2015), suggest that at the time where compressional forces arise in a high angle within a slow spreading mid-oceanic ridge, detachment faults parallel and close to the ridge can be inverted. This process can create intra-oceanic subduction zones even if the oceanic crust is still young, weak and not very dense.
2. It has been also proposed that geological features like a transform/ fracture zone in the right position separates oceanic plates of contrasting ages. (Robert J. Stern, 2004). Numerical modeling results have predict that these features can create a weak zone where the old oceanic lithosphere can initiate subduction spontaneously (Gerya, Connolly, & Yuen, 2008; Ksenia Nikolaeva, Gerya, & Connolly, 2008; Zhu et al., 2009). It is believed that the new Eocene subduction zones along the western edge of the Pacific plate are associated with this hypothesis. (Robert J. Stern, 2004).

Therefore, heterogeneities in the oceanic lithosphere such as variation in rheology in the crustal layers or inheritance can favor intra-oceanic subduction. However, for realistic weak zones, it is poorly understood what is the grade of their influence regarding to different ages of oceanic lithosphere and lithospheric thicknesses.

1.2 Oceanic core complexes and serpentinisation

Slow and ultraslow spreading ridges are associated with the development of low angle detachment faults with big offsets to accommodate the divergence(Maffione et al., 2015). These structures allow the exposure of upper mantle and lower crust rocks at the surface and thus the formation of Oceanic Core Complexes (OCC) (Figure 1.2) (Garcees & Gee, 2007; C. J. MacLeod, Carlut, Escartín, Horen, & Morris, 2011; Morris et al., 2009; Sauter et al., 2013; Smith, Escartín, Schouten, & Cann, 2008; Whitney, Teyssier, Rey, & Buck, 2013). The detachment faults usually form close to an oceanic ridge and parallel to its axis (Escartín et al., 2008; Smith, Cann, & Escartín, 2006; Smith et al., 2008). The width of the exposed surface of the footwall of these detachment faults can be occasionally longer than 100km, as for example the Godzilla Megamullion (Ohara et al. 2001). Seawater can penetrate crust and circulate in grater depths in the oceanic lithosphere where the permeability is initially low (Escartín et al., 2008; Reston & Ranero, 2011), triggering the hydrothermal alternation (serpentinisation) of the exhumated rocks (Andreani et al., 2014; Bach, Garrido, Paulick, Harvey, & Rosner, 2004; Bach et al., 2006; Beard et al., 2009; Boschi et al., 2013; Boschi, Früh-Green, Delacour, Karson, & Kelley, 2006; Klein et al., 2009; Maffione, Morris, Plümper, & van Hinsbergen, 2014; Mével, 2003; Plümper, Beinlich, Bach, Janots, & Austrheim, 2014; Plümper, Røyne, Magrasó, & Jamtveit, 2012; Schroeder, John, & Frost, 2002)

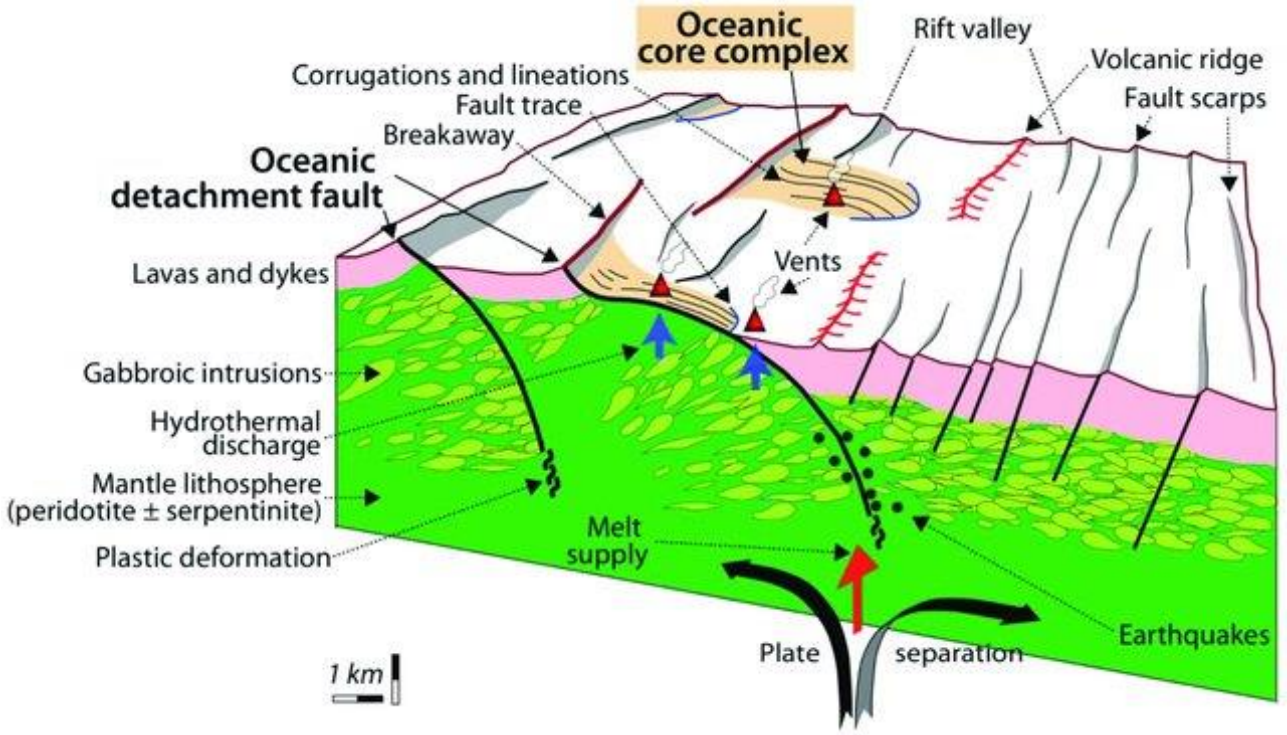

Figure 1.2 Schematic representation of the structure of an oceanic lithosphere close to a slow spreading mid-oceanic ridge shows the formation of Oceanic detachment fault which are associated with OCCs and the hydrothermal activity causing hydro-alternation (serpentinisation) of mantle peridotites.

Serpentinisation of the exposed mantle rocks significantly weakens the oceanic lithosphere. The hydrothermal circulation is responsible for the formation of serpentine minerals which are considerably weaker than the unaltered mantle rocks, the strength of which can be at least one order of magnitude (Escartin, Hirth, & Evans, 1997; C. J. MacLeod et al., 2002) and they also display low friction coefficient (μ=0,15-0,45) (Escartin et al., 1997). It is known from observations that the serpentinite zone can be extended up to 10km-12km deep (Bayrakci et al., 2016), while the density of the serpentinites referred to be 2600kg/m3 (Escartin et al., 1997). Studies on rock mechanics and rheology of serpentinized peridotites (eg. Escartin, Hirth, & Evans, 2001) have shown that even incipient serpentinisation of the oceanic crust (9%-15%) can decrease significantly the overall strength of the lithosphere and support strain localisation for long periods of time.

1.3 Fracture zone and Transform faults

Transform faults are structures in the oceanic lithosphere that exist next to ridge segments, translating the ridge from tens up to 100 km (P. J. Fox et al., 1984; C. DeMets, et al., 2010). The offset of transform faults or fracture zones can be significant enough to bring two oceanic lithospheres with different densities, thickness and seafloor elevation the one next to the other (Stern, R.J, 2004). Numerical models on the spontaneous nucleation of subduction zones have shown that these structures could have been responsible for the formation of intra-oceanic subduction arcs such as Izu-Bonin-Mariana forearc (R.J. Stern, et al., 1992; J.H. Natland et al., 1981; J.W. Hawkins et al., 1984). In that sense these faults can create weaknesses in the oceanic crust that are enough to overcome the lithospheric strength allowing the spontaneous sinking of the oceanic lithosphere (Stern 2004).

2 ANALOGUE MODELS

2.1 Model concept and set-up

The presence of a passive margin has shown an important role for localizing deformation governed by the strength contrast between continental and oceanic crust (Auzemery et al. 2019, in revision). This study aims to identify favourable parameter combinations for subduction initiation in the oceanic domain and to define patterns of tectonic deformation. The presence of a weak zone in oceanic domains can be explained by geological inherited processes such as exhumation and serpentinisation of mantle peridotites (Grevemeyer 2018). Such a heterogeneity with smaller density than the rest of the oceanic crust causing of a relatively reduced overall strength of the lithosphere under the location of the weak zone, and hence of the yield stress.

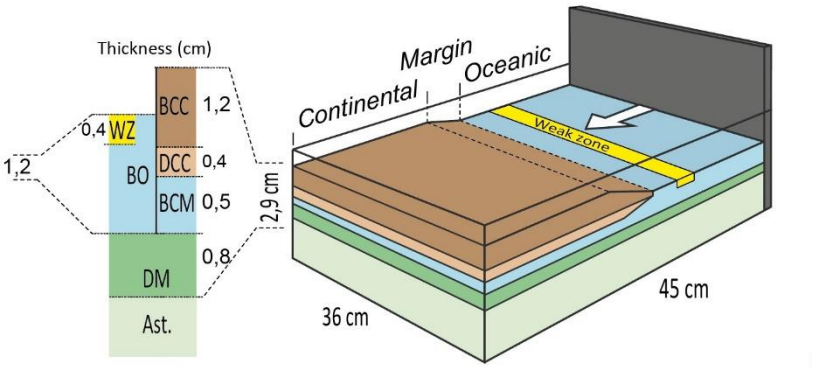

Figure 2.1 Experimental set-up incorporating a continental and an oceanic domain separated by a 5cm long passive margin over a high-density and low-viscosity liquid representing the asthenospheric mantle. A weak zone has been integrated in the oceanic domain. The white arrow indicates the direction of the moving wall which is 0.5 cm/hr

In line with passive margin geometries (2.1), the experiments consist of both continental and oceanic lithospheres which are separated by a wedge-shaped margin simulating the necking zone of the passive margin. The model's continental crust consists of a 4-layer set up with an upper brittle crust and a ductile crust being 12mm (36 km in nature) and 4mm (12 km in nature) thick respectively and below there is the subcontinental mantle consisting of an upper brittle layer and a lower ductile one of 5mm and 8mm respectively. At the area of the margin, both brittle and ductile continental crustal layers thin towards the oceanic domain.

The oceanic brittle lithosphere has a thickness that varies to represent different ages. According to numerical modelling studies (Burov, 2011) the brittle ductile transition for a mature lithosphere is

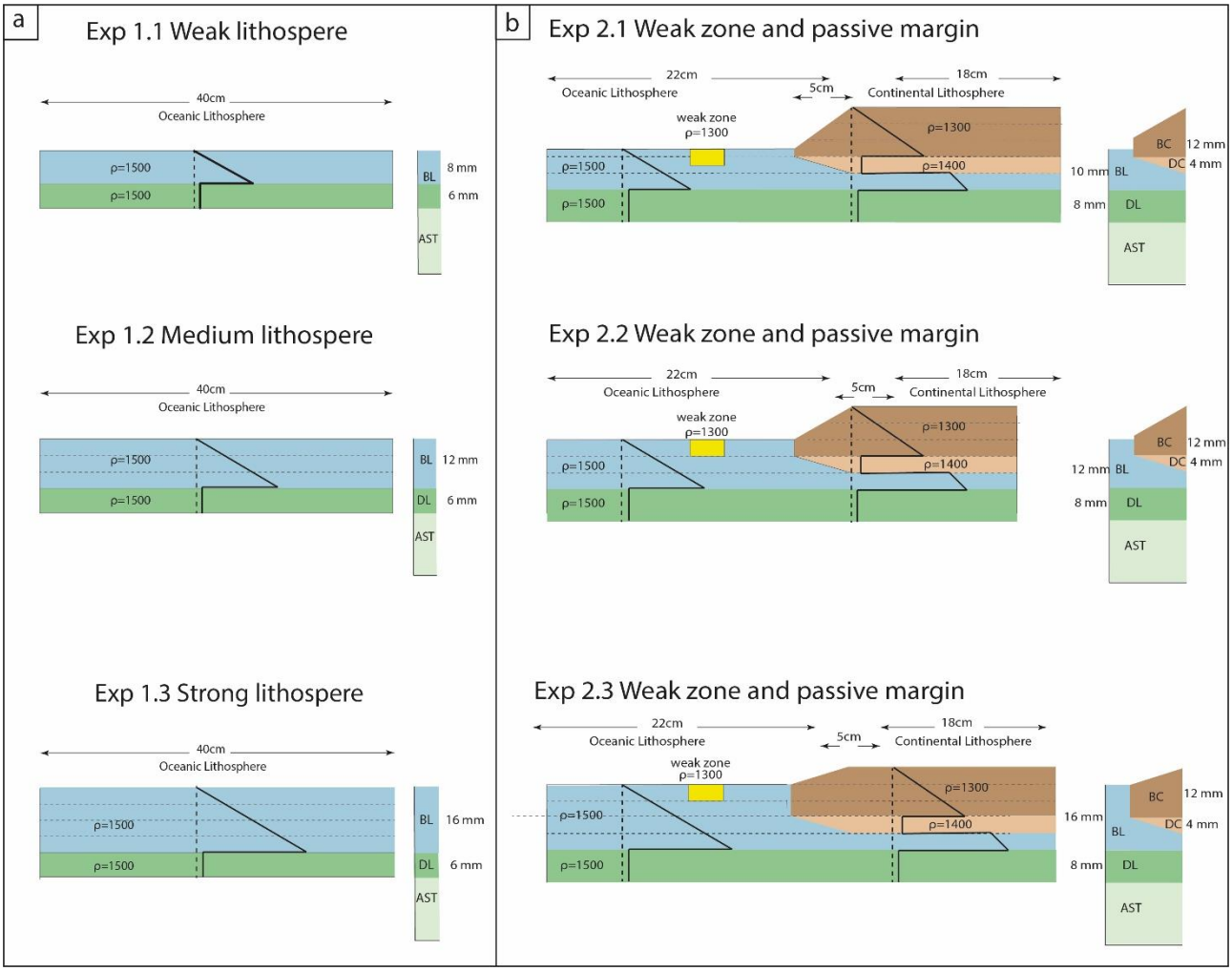

Figure 2.2 a) Representation of a cross-section for experimental set 1. b) Representation of a cross-section for experimental set 2. The thick black lines show the strength profile for each experiment. The vertical axis and horizontal axis are not in the same scale. The height of each set up is exaggerated for illustrational purposes.

located around 36 km below the surface, for an old can be deeper than 45km and at 25 km depth for a young one. Therefore, the model's brittle oceanic lithosphere varies from 8mm to 16mm.

The ductile oceanic mantle maintains its thickness (8mm) under both oceanic and continental crust. Oceanic crust incorporates a thin narrow zone of less dense material parallel to the passive margin. This zone corresponds to a 4mm layer of feldspar sand which represents a compositional heterogeneity in the first 12 km of the oceanic lithosphere.

The lithospheric set up as described above, has been scaled down to meet analogue modelling constraints. Therefore, the conducted experiments were placed in a plexiglass tank of a 36cm*45cm surface area and 15cm height with a moving wall on one side. This scales to an area of 1200km-1500km

by 1080km, applying a scaling ratio of 3km per cm. The moving wall is attached to an electric engine which provides the horizontal motion to the wall representing the mid-oceanic ridge push. The tank is filled with a liquid mixture of glycerol and sodium polytungstate solution representing the asthenospheric mantle.

The first set of lithospheric models consist solely of oceanic lithosphere (Figure 2.2a) whereas the second set incorporates a 5 cm long passive margin. For the first set of experiments a constant thickness of 8 mm has been considered for the ductile oceanic layer and variable thicknesses for the brittle layer.

In the second set *(*Figure 2.2*b)* of models (involving a passive margin and a weak zone), the continental domain has a total length of 23 cm and consist a thinned (5 cm) and an un-thinned part (18 cm). A slope of 5^{o} towards the oceanic domain has been applied as a result of the thicker continental lithosphere. The length of the margin is 5 cm in the models, an equivalent of 150 km in nature (this is slightly less than the average). A weaker zone in the oceanic domain, has been simulated in the oceanic crust by implementing a 4mm thin and 3-4cm wide zone of feldspar sand (2.3).Figure 2.2b). The thickness of the brittle oceanic lithosphere varies from 10mm to 16mm while the thickness of the brittle continental lithosphere remains the same (12mm) for every model.

2.2 Methods

The following methodology adopted for the analysis of each experiment. The spatial and temporal deformation occurrence is analysed by using surface evolution models and a cross section at the end of experiments. The surface evolution is monitored using digital repeat photography and laser scans (every 30 minutes) at the surface of the models. The final lithospheric deformation patterns are retrieved by cutting each experiment and photographing representative vertical cross-sections. The laser scans have been converted to digital elevation models and combined with the cross-sections in order to build a 3-D lithospheric scale models.

2.3 Model Materials

For the natural rocks φ=30° and C=50MPa (Byerlee, 1978). The materials to simulate brittle oceanic and continental lithosphere are aeolian quartz and feldspar sand respectively. These materials have both φ=22°-35° and C=40Pa as they have been determined with ring-shear experiments in the Tectonic Laboratory in Utrecht and at the GFZ in Postdam. Mixtures of silicon putty have been used for the ductile regimes of the models. The viscosity and the densities of the silicon putties have been measured using a coni-cylindrical viscometer and a pycnometer in the Tectonic Laboratory in Utrecht. The exact parameters of the materials are shown in Table 1. The densities in the models are scaled according to natural differences between oceanic and continental crusts. An average density between 3300 kg/m^3 and 3380 kg/m^3 for oceanic lithosphere and 2850 kg/m^3 for a continental lithosphere has been chosen for this study. Additionally, the viscosity of the ductile mantle has been determined according to studies using both diffusion and dislocation creep flow laws (Billen & Hirth, 2005; Hirth & Kohlstedt, 2003; van Hunen, Zhong, Shapiro, & Ritzwoller, 2005; Watts & Zhong, 2000) in accordance with field observations

Table 1 Rheological Parameters for the analogue materials used in the experiments

Layer	Material	Density ρ (kg/m^3)	Coefficient Friction μ	Viscosity η (Pa s)	Stress Exponent n
Brittle Continental Crust (BCC)	Feldspar sand	1300	0,4-0,7		
Ductile Continental Crust (DCC)	Rhodorsil Gomme + sand mixture			4.54E+04	1
Brittle Continental Mantle (BCM)	Quartz sand	1500	0,6		
Brittle oceanic lithosphere (BO)	Quartz sand	1500	0,6		
Ductile Lithospheric Mantle, medium (DM)	Rhodorsil Gomme + sand mixture	1500		4.13E+04	1.05
Asthenospheric Mantle	Polytungstate + glycerol	1470			

(Bills, Currey, & Marshall, 1994; Kaufmann & Amelung, 2000; Vergnolle, Pollitz, & Calais, 2003) or glacier rebound models (Lambeck, Smither, & Johnston, 1998; Mitrovica & Forte, 1997).

2.4 Scaling

Analogue models must be adequately scaled to simulate the processes and the developing structures of natural prototypes accurately. As a result, the models have to be geometrically, kinematically and dynamically similar to the natural example.

The geometrical similarity for the models accomplished by applying a length scale ($L^*=L_m/L_n$) factor of $L^*= 3{,}33.\ 10^{-7}$ where the exponent * refers to the ratio between model and prototype (Brun, 2002). Therefor 1 cm corresponds to 33 km in nature. These experiments have been shortened by 10 cm which is equal to ~330 km in the nature.

To ensure dynamic similarity, the Reynolds number has been calculated. According to (Schellart & Strak, 2016), the Re in the natural flows is very small ($Re<10^{-20}$). In the experiments the Re value is much smaller than 1 (*Table* 2), which means that inertial forces are insignificant in comparison to the viscous ones. In this sense, the scaling of different kind of forces can deviate from absolute dynamic similarity. Hence, length ratios and time ratios can be independent variables (Ramberg, 1981). Although inertial forces are negligible, ratios between frictional, viscous and gravitational forces ratios must be constant.

Table 2 Scaling parameters

Layer		Thickness (m)	Density ρ (kg/m3)	Viscosity η (Pa s)	Sm	Rm	Re
Brittle Continental Crust (BCC)	model	0.008	1300		1.120		
	nature	24000	2850		1.428		
Ductile Continental Crust (DCC)	model	0.004	1400	4.54E+04		1.76	1.71E-10
	nature	12000	3100	1.00E+21		1.74	3.78E-24
Brittle Continental Mantle (BCM)	model	0.005	1500		0.992		
	nature	15000	3300		1.425		
Brittle oceanic, weak (BO)	model	0.010	1500		1.244		
	nature	30000	3200		1.429		
Brittle oceanic, medium (BO)	model	0.012	1500		1.299		
	nature	36000	3200		1.429		
Brittle oceanic, strong (BO)	model	0.016	1500		1.375		
	nature	48000	3200		1.429		
Ductile Lithospheric Mantle (DM)	model	0.008	1530	4.13E+04		8.641	4.25E-10
	nature	24000	3350	3.00E+21		8.630	9.53E-24
Asthenospheric Mantle			1475	1.5			

The dynamic similarity for Mohr-Coulomb materials is given by the relation $\sigma^*=p^*g^*l^*$ where ρ, g, l, the density, gravitational acceleration and thickness respectively (asterisk* represent the model/prototype ratio). The experiments conducted under normal gravitational acceleration, thus $g^*=1$. Density ratio for

the brittle crust is ρ*=0.45 since the brittle lithosphere density (ρ) is 2850 and 3300 kg/m^3 for the continental and oceanic crust respectively, and the sands we used have densities of 1300 kg/m^3 and 1500 kg/m^3. Subsequently the stress ratio is σ*=1,55*10^{-7}. Brittle layers are described by frictional behaviour with a shear stress to increase linearly with the depth by the Mohr-Coulomb relationship:

$$\tau = C + \sigma(\tan\varphi),$$

where τ is the shear stress, C the cohesion, ϕ the angle of friction, and σ the normal stress and is independent of the strain rate. From the Mohr circle (for more details, see (Jaeger & GoW, 1979)), Therefore, in compression where the vertical stress $\sigma_v = \sigma_3 = \rho g z$, and for φ=30^o, the maximum differential stresses in models is given by:

$$\sigma_1 - \sigma_3 = 2 \cdot \rho \cdot g \cdot z,$$

where σ_1 and σ_3 are the maximum and minimum principal stresses and z the depth.

Dynamic and kinematic similarity for the ductile layers can be tested by the Ramberg number (Rm). Rm is the ratio (Weijermars, 1986) between gravitational and viscous forces and is given by the relationship:

$$\mathrm{Rm} = \frac{\rho g h}{(\sigma_1 - \sigma_3) viscus}$$

Where ρ and h is the density and thickness of the viscous layer and g the gravitational acceleration. In order to fulfil the dynamic similarity for the viscous layer the Rm for the model and for the prototype must be equal.

The silicon putties that have been used vary in density and viscosities and most of their properties meet the desired requirements except of the very high viscosity for stress exponents over 3 even at the smallest strain rate (Davy & Cobbold, 1991). To solve this problem, nearly Newtonian putties were used. The putties, despite they deviate from power flow law in the upper lithospheric mantle, approximate well the total strength of the ductile lithospheric mantle (Drury, 2005). The ductile layer's strength is given by the following equation which links the stresses with the strain rate (τ) (e.g.(Kirby, 1985; Weertman, 1978):

$$\sigma_1 - \sigma_3 = 2 \cdot \tau \quad \text{and} \quad \tau_{(n)} = 2 \cdot \eta \cdot \dot{\gamma}$$

Where η is the effective viscosity, $\dot{\gamma}$ the shear strain rate and n the flow behaviour index. The shear strain rate is difficult to estimate in advance because it depends on the number of faults that are going to form in the model (Midtkandal, Brun, Gabrielsen, & Huismans, 2013). However, the shear strain rate $\dot{\gamma}$ can be expressed as ratio between model's horizontal velocity of deformation V and the known thickness of the

ductile layer h. Therefore, to represent a ductile layer with a given thickness and viscosity, the differential stress is given by (Nalpas & Brun, 1993; Smit, Brun, & Sokoutis, 2003):

$$\dot{\gamma} = \frac{V}{h} \qquad \text{and} \qquad \sigma_1 - \sigma_3 = 2 \cdot \eta \cdot \frac{V}{h}$$

Finally, the time was scaled in respect to the length ratio and the natural evolution time of approximately 25My. This time corresponds to 20 hours of the experiment and yields to a time ratio of 8.38E-11 and hence to a convergence rate of 0.5 cm/hr representing 1 cm/yr in nature.

2.5 Assumptions and simplifications

In this study, the lithospheric scale model's layering has been approached according to a simplified rheological stratification of the lithosphere. Considering this, the representation of ductile layers using homogenous viscous materials has been adopted as a first order approximation (Davy & Cobbold, 1991). The thickness of the viscous layers is uniform. The conducted experiments deformed under a constant convergence rate. The shortening of each model is the result of a horizontal moving wall and the subduction initiates by the force that this wall applies (representing forces in the nature like ridge push) and not by spontaneous sinking of the lithosphere. No temperature variation with the depth is applicable to the models. Consequently, the rheological properties of the ductile layers of the models, which are strongly depended on temperature in the nature (Brace & Kohlstedt, 1980; Ranalli, 1995), are uniform and independent of depth. Although the temperature depended viscosities have been taken into consideration for the model set up. Temperature is constant during deformation as well. Only the mechanically significant part of the mantle lithosphere has been taken into account, therefore the limit with the asthenospheric liquid is not representative of the observed lithosphere-asthenosphere boundary. No erosion or sedimentation that can lead to load redistribution has been considered, as loading from sediments is not sufficient to influence subduction (Cloetingh et al 1989) . Despite the simplifications and the analogue modelling limitations, the tectonic behaviour of a locally weakened oceanic lithosphere converging with a continental one can be simulated and provide first-order deformation patterns and the associated topography.

3 EXPERIMENTAL RESULTS

Considering the modelling assumptions and limitation explained above, a series of analogue experiments have been performed and interpreted. In this section the results of the shortening of oceanic lithosphere will be presented by analysing the final deformational structures of the 3D lithospheric models for each experiment and the evolution of deformation through time using the surface elevation models and the topographic profiles. Taking in consideration the initial parameters assumed for each analogue model, the forces (as they specify in section 0) have been calculated for each experiment using a matlab script.

3.1 Analogue experiments

3.1.1 Set 1: Oceanic lithosphere

Experiment 1.1 corresponds to a young and thin oceanic lithosphere with a brittle layer thickness of 8mm (Figure 3.1 Illustration of representative cross sections and the final topography for experiments 1.1 (a) , Exp 1.1). No deformation structures have been developed on the surface of the model and no failure of the crust has occurred during the experiment. The topographic evolution of the surface shows that the model responded to the shortening by approximately 1mm of uplift and by developing a 15cm wave-length and short amplitude lithospheric folding. Additionally, a 2.1mm thickening of viscous lithosphere is observed.

Experiment 1.2 with an oceanic brittle thickness of 12mm (Exp1.2), responds to shortening in a similar way as experiment 1.1 and lithospheric folding and thickening of the ductile layer by 6.5mm lead to surface uplift up to 1.5mm. A 5mm topographic bulging, consequence of a pop-up structure of the oceanic crust, is observed on the left side of the model close to the fixed wall of the tank. The 5mm uplift is accommodated by two opposite verging fore-and back-thrusts and is considered as a boundary effect of the proximate tank wall.

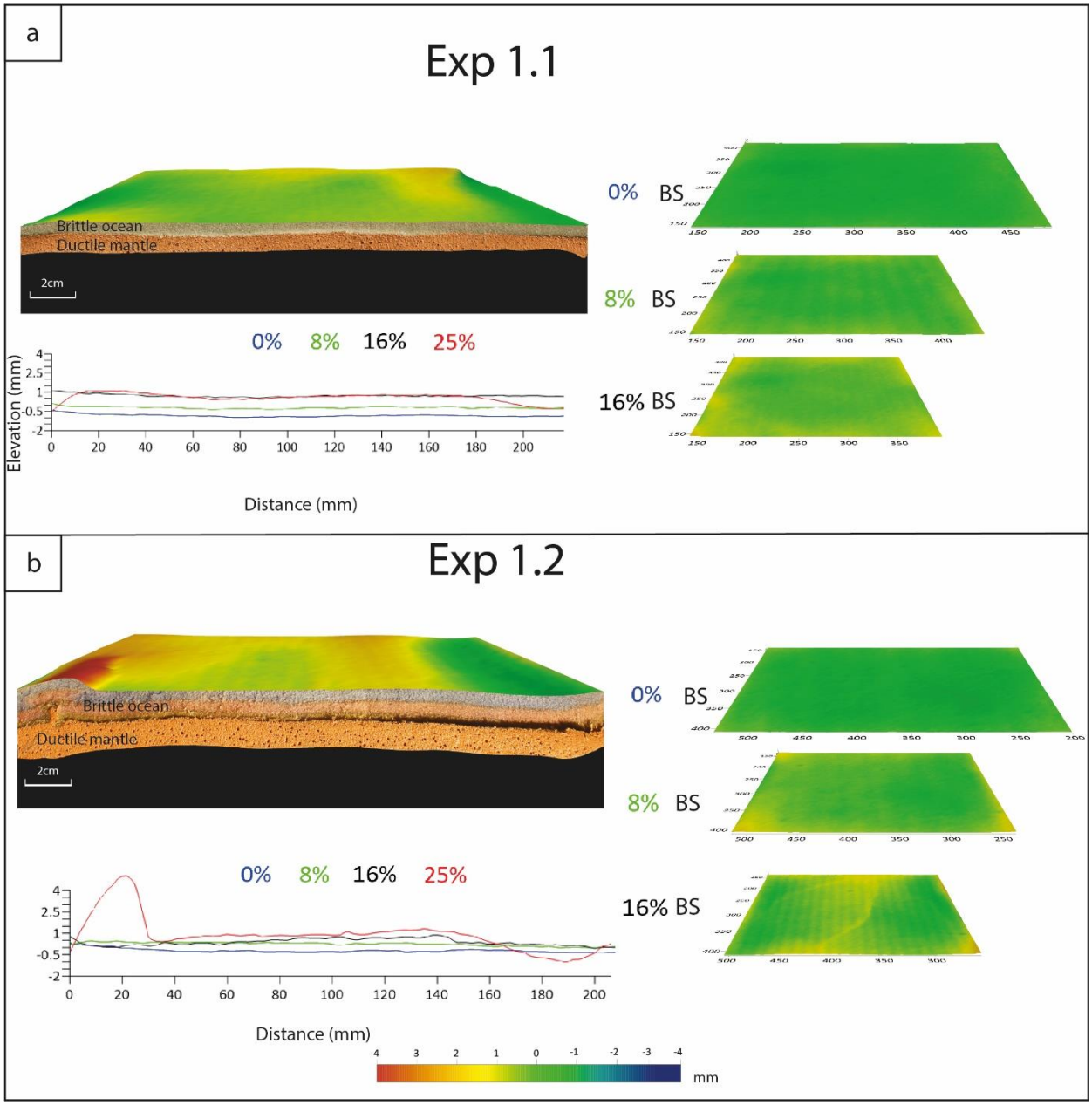

Figure 3.1 Illustration of representative cross sections and the final topography for experiments 1.1 (a) and 1.2 (b) testing a weak and a moderate oceanic lithosphere respectively after 25% of BS. The 3 snapshots of the surface elevation on the right side of each experiment, are demonstrating from top to bottom the evolution of the model's topography from 0% of BS until 16% of BS. The topographic evolution is also demonstrated in the diagrams below each model where the vertical axis is not in the same scale as the horizontal one, but it is exaggerated to illustrate clearly the elevation changes during the experiment.

Experiment 1.3 involves a strong oceanic crust with a thickness of the brittle layer of 16mm (Figure 3.2, Exp1.3). As in experiments 1.1 and 1.2, no crustal failure occurred during shortening. Instead, a 20cm wave-length folding of the lithosphere has been observed.

Experiment 1.4 corresponds to a moderate strength oceanic lithosphere with a brittle layer thickness of 12mm and a weak zone of 4mm in the middle (Figure 3.2. Exp1.4). Similar to the previous

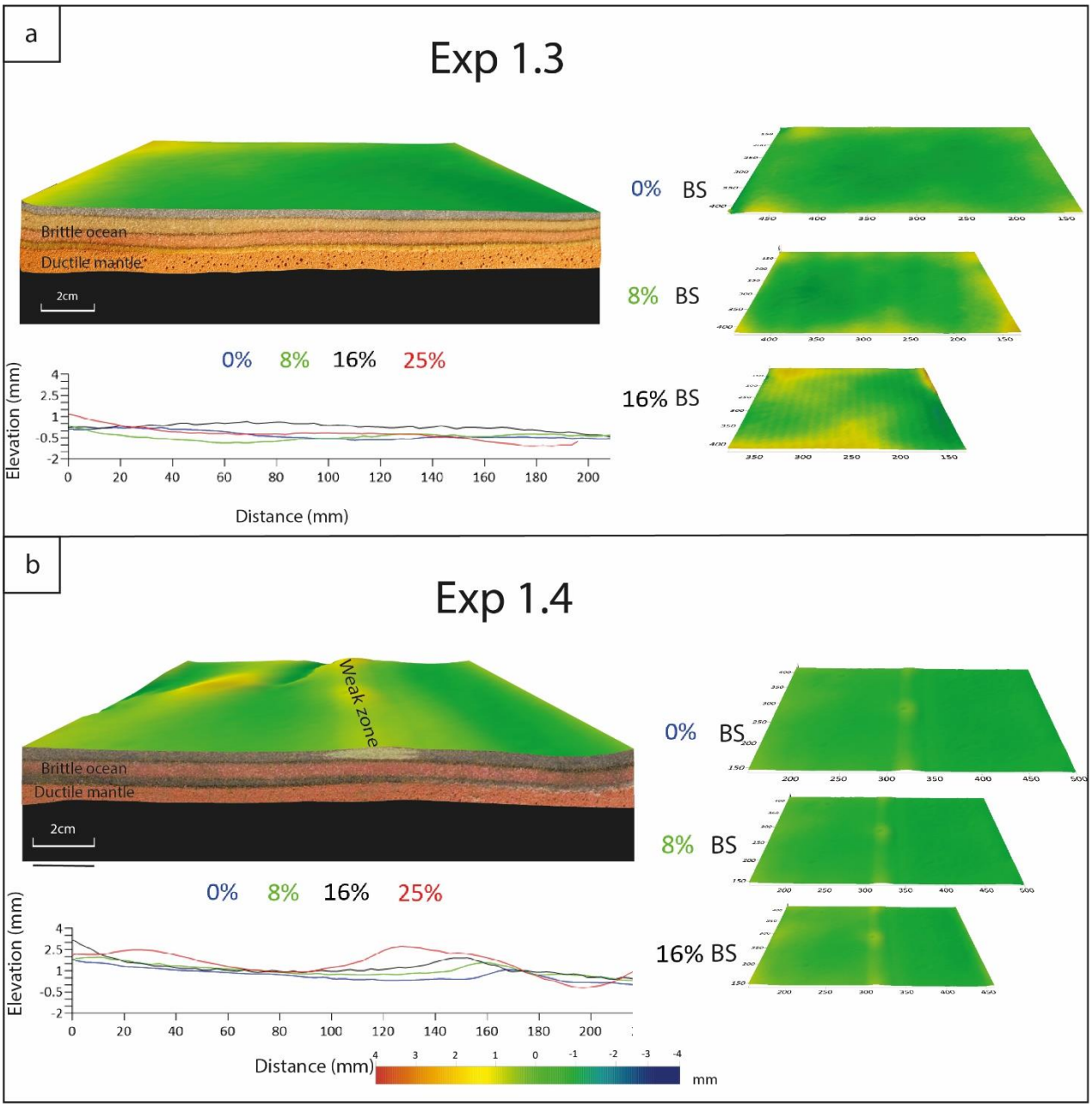

Figure 3.2 Illustration of representative cross sections and the final topography for experiments 1.3 (a) and 1.4 (b) testing a weak and a moderate oceanic lithosphere respectively after 25% of BS. The 3 snapshots of the surface elevation on the right side of each experiment, are demonstrating from top to bottom the evolution of the model's topography from 0% of BS until 16% of BS. The topographic evolution is also demonstrated in the diagrams below each model where the vertical axis is not in the same scale as the horizontal one, but it is exaggerated to illustrate clearly the elevation changes during the experiment.

experiments, the brittle oceanic layers follow the viscous mantle folding without brittle deformation occurring.

In all the experiments, no rupture of the crust has been observed but some boundary deformation occurs on each edge of the model. The total shortening expressed by a gentle long wave-length folding of the

lithospheres and a general uplift of the surface of a few mm. The same results are obtained also for the last model with the weak-zone.

3.1.2 Set 2: Weak zone in the oceanic lithosphere

The models of set 2 consist of an oceanic and a continental domain and involve a weak zone in the oceanic crust, which is the main variable of set 2 experiments.

Experiment 2.1 corresponds to a weak oceanic lithosphere including a rectangular weak zone parallel to the ocean continent boundary (Figure 3.3, Exp 2.1). After 7% of bulk shortening, the passive margin starts to deform. Two very shallow, crustal scale, opposite verging fore and back-thrusts form parallel to the boundary of continental and oceanic domains to accommodate the deformation. These faults remain active for a short time creating an 1mm uplift of the surface. Shortly after the passive margin's faults deactivation, deformation localises at the weak zone where the oceanic crust breaks parallel to this heterogeneity. After a bulk shortening of approximately 10%, the bending of the under-thrusting oceanic domain progressively forms a shallow trench. Rupture of the oceanic domain occurs at 12% of bulk shortening. A fore-thrust, parallel to the weak zone, forms across the model forcing the oceanic crust to thrust under the weak zone. This lithospheric scale feature stays active until the end of the experiment propagating progressively to the lithospheric mantle. It accommodates the shortening leads to intra-oceanic subduction, creating a shallow slab with a subduction angle of 25^{o}. Accretion of the crust results in a narrow (2.5cm width) zone of surface deformation with strong topographic uplift of about 7-8mm at the location of the weak zone.

Experiment 2.2 is has a moderate strength oceanic lithosphere (Figure 3.3, Exp. 2.2). The increased strength of the oceanic brittle lithosphere changes the deformation patterns and the timing of the events in this experiment. However, the relative sequence of occurrence of the deformational episodes (eg deformation of the weak zone follows the deformation of the PM) is the same as in the experiment 2.1. Quickly after the initiation of the experiment, after of 7% bulk shortening, local deformation and uplift at the ocean-continent transition (OCT) occurs. Similar to experiment 2.1, failure of the oceanic crust at the weak zone succeeds the inactivation of OCT's deformation. The trusts that accommodated the deformation of the OCT have not preserved due to oceanic obduction, so they are not visible in the cross section. At 12% of bulk shortening, a low angle, fore-thrust forms parallel to the weak zone (fault 1). It creates a trench in the oceanic domain and under-thrusting develops oceanward. The hanging block propagates continent-wards over the oceanic crust, which results in a 3cm-4cm wide zone with a strong topographic uplift (up to 5mm height) and the formation of a narrow but deep trench on the front of the overriding plate, as the topographic profile clearly illustrates at 15% of bulk shortening (Figure 3.3b). At this step, the oceanic lithosphere is deflected downwards. Subsequently, the overriding oceanic plate

covers the trench and at 20% of bulk shortening reaches the continental margin. Obduction of the oceanic crust takes place late in the experiment. The resistance of the strong continent slows down the obducting ocean causing further deformation of the oceanic crust in the form of a back-thrust (fault 2). At the same time, the main thrust (fault 1) is being inactivated. At this point, the continental crust deforms (thrust faults 3 and 4) by the propagating oceanic domain and blocks further development of the obduction. The polarity of the slab during under-thrusting is ocean-ward.

Experiment 2.3 represents a strong/mature oceanic crust in convergence with a strong continent (Figure 3.3, Exp 2.3). In this set up, the oceanic crust remains undeformed during almost all the experiment. Much of the deformation in the model occurs at the ocean-continent boundary giving rise to a wider (comparing to experiment 2.2) triangular pop-up structure of around 3mm. A pair of opposite verging back and fore-thrusts accommodates the deformation of the margin from the beginning of the experiment until 15% of bulk shortening is reached. Further deformation and failure of the oceanic lithosphere is not observed until 18% of BS when oceanic lithosphere breaks parallel to the weak zone. A back-thrust (fault 3) forms to accommodate the deformation at the weak zone. The activation of this fault allows the under-thrusting of the oceanic plate, enabling subduction initiation at the late stages of the experiment. The polarity of the slab of under-thrusting is ocean-ward. A 3mm uplift of the hanging wall in a 2 cm wide zone along the weak zone is the immediate topographic response to the subduction. A second opposite verging thrust (fault 4) forms and changes the polarity of the subduction at 20% of BS. The new formed fore-thrust deactivates, cuts and bends the back-thrust creating the final geometry, which resembles that of pop-downs bounded by opposite verging fore- and back-thrusts (Sokoutis, Burg, Bonini, Corti, & Cloetingh, 2005).

In all experiments, limited deformation starts at the passive margin and the subsequent intra-oceanic rupture of the crust at the location of the weak zone is followed by under-thrusting. In weak and moderate strength oceanic lithosphere, the main thrust remains active until the end of the experiments. The trench forms parallel to the rupture zone because of the under-thrusting of the lithosphere while high topography develops on the hanging wall of the thrust. On the other hand, a strong oceanic brittle lithosphere causes more extensive deformation and uplift at the passive margin while fracture in to the oceanic domain occurs at the end with the main thrust remaining active for a short time and an opposite verging second thrust reverses the polarity of the subduction. The polarity of the slab during under-thrusting is ocean-ward in experiment 2.2 and continental-ward in experiment 2.3. Obduction of the oceanic lithosphere is observed in experiment 2.2 after 20% of bulk shortening. However, the geometry of the weak zone has not been set to control subduction direction. The polarity of the subduction is probably controlled by very small-scale (geometrical imperfections at the weak zone during the building process of the experiments) heterogeneities due to experimental errors.

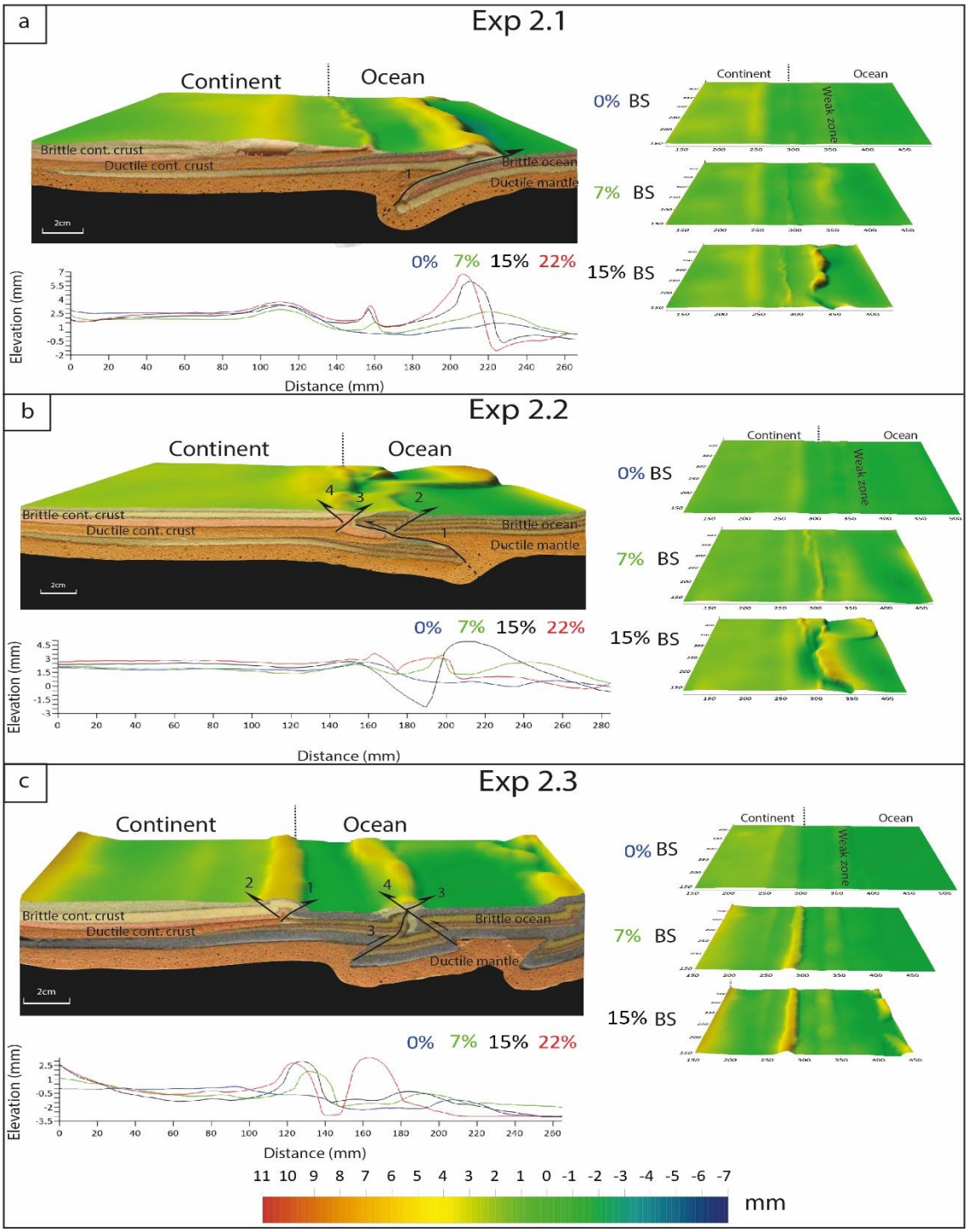

Figure 3.3 Illustration of representative cross sections and the final topography for experiments 2.1 (a), 2.2 (b) and 2.3 (c) testing a weak and a moderate and old oceanic lithosphere respectively after 22% of BS. The 3 snapshots of the surface elevation on the right side of each experiment, are demonstrating from top to bottom the evolution of the model's topography from 0% of BS until 15% of BS. The topographic evolution is also demonstrated in the diagrams below each model where the vertical axis is not in the same scale as the horizontal one, but it is exaggerated to illustrate clearly the elevation changes during the experiment.

3.2 Quantification of forces

For a better understanding of the role of the vertical (buoyancy and viscous resistance forces) and horizontal forces that drive deformation, two dimensionless numbers are calculated: F1 (1) which is the ratio between the buoyancy forces of the crust against the viscous resistance of the ductile mantle (ση) and F2 (2) which is the ratio between the integrated strength of oceanic crust (σo) over the integrated strength of the continental crust (σc). F1 and F2 are calculated from the following equations:

$$F1 = \frac{Buoyancy\ force}{Viscous\ resistance} = \frac{\sigma\rho}{\sigma\eta} = \frac{(\rho\ Lith - \rho\ Asth)\cdot g\cdot h\ Lith}{\eta\cdot\dot{\varepsilon}} \quad (1)$$

and

$$F2 = \frac{\sigma o}{\sigma c} = \frac{\int_0^{moho}(\sigma 1-\sigma 2)dz\ (ocean)}{\int_0^{moho}(\sigma 1-\sigma 2)dz\ (continent)} \quad (2)$$

where ρ, g, h, $\dot{\varepsilon}$ and η is the density, the gravitational acceleration, the thickness, the strain rate and the viscosity respectively. F2 is calculated by integrating the strength from the surface to a constant depth, which correspond to the continental Moho, both for the continent and the ocean. This simplification is made to understand the horizontal forces in the crust at the OCB. F2 is calculated without taking into consideration the isostatic equilibrium. Therefore, the numerical simulations of the experiments below, show the initial rheological conditions of the experiments that incorporate a passive margin.

For each of the models of experimental set 2, a graph of the force equilibrium and total strength along the model has been produced. An overview of the integrated strength in the lithosphere along with the buoyancy number F1 and the horizontal force ratio F2 is presented below.

Experiment 2.1: The total strength of the crust as it is illustrated in Figure 3.4a shows that the weakest part of the crust is located at the weak zone. In this scenario buoyance number F1 at the ocean continent margin is 0.78 (<1) and -0.04 at the weak zone (Figure 3.4b). It means that in the oceanic lithosphere, the buoyancy force is less than the ductile resistance of the lithospheric mantle. Without the implementation of weak zone, deformation would occur at passive margin. F2 has a value of 1.01 at the passive margin whereas at the weak zone has a value of 1.1. This difference in rheology is enough to initiate deformation in the ocean such as in the analogue experiment. It is controlled by the strength difference between the lithospheres in the oceanic domain and at the weak zone. This difference initiates the rupture of the brittle lithosphere, the deflection and consequently the under-thrusting in oceanic domain.

Experiment 2.2: In this set up the total integrated strength increases (Figure 3.4d) as the set up represents an older and thicker oceanic lithosphere. A small drop of the integrated strength in the weak zone location reflects the effect that the smaller density of the first few mm (the fs sand of the weak zone) has to the overall stress at the lithosphere underneath the zone. A secondary drop at the OCB occurs due to the higher strength contrast between Oceanic and continental domains. The F1 Figure 3.4e) is now >1 (0.81) thus the negative buoyancy of the crust is superior than the viscous resistance of the mantle. As in experiment 2.1, F2 (Figure 3.4f) at the passive margin is >1 (1.06) but still smaller than the F2 at the weak zone which has a value of 1.09.

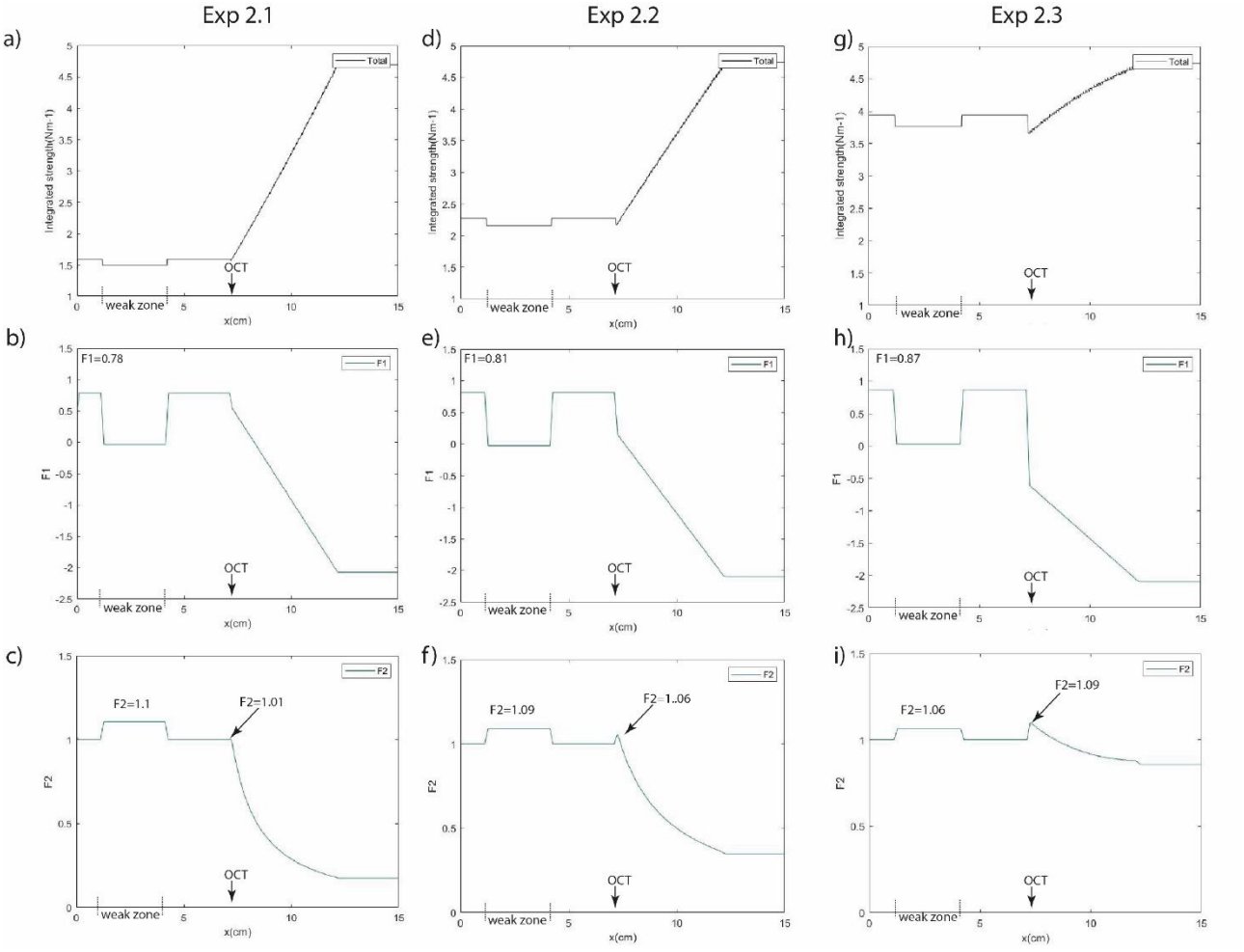

Figure 3.4 a,d,g) Total integrated strength for experiments 2.1, 2.2 and 2.3. b,e,h) Buoyancy number F1 for experiments 2.1, 2.2 and 2.3. c,f,i) Strength contrast F2 for experiments 2.1, 2.2 and 2.3. The OCT and the weak zone locations are shown at the horizontal axis of each diagram. The continental domain is located right of the OCT whereas the oceanic one is located at the left of the OCT.

Experiment 2.3: This model corresponds to a strong and mature oceanic lithosphere and as shown on the graph of Figure 3.4g. In this graph the total strength reduces sharply at the weak zone as well as at the OCB, reflecting two weak points in both locations. F1 at the oceanic domain is 0.87 and 0.03 at the

weak zone. In both locations F1 is increased comparing to the previous experiments as a result of the thickness increase of the brittle ocean. F2 shows also increased values in comparison with Experiment 2.2 for both the weak zone and OCB (1.06 and 1.1 respectively)

4 DISCUSSION

With slow spreading velocity field at mid-oceanic ridges, several core complexes and detachment faults can be formed. It can produce mantle exhumation leading to hydration and serpentinization (Guilott et al., 2015) of the first 7km-12km of the mantle lithosphere(Dick, Lin, & Schouten, 2003; Escartín et al., 2008; C. MacLeod et al., 2009; C. J. MacLeod et al., 2002)

It has been shown that the localization of deformation and thus of evolving subduction zones is strongly

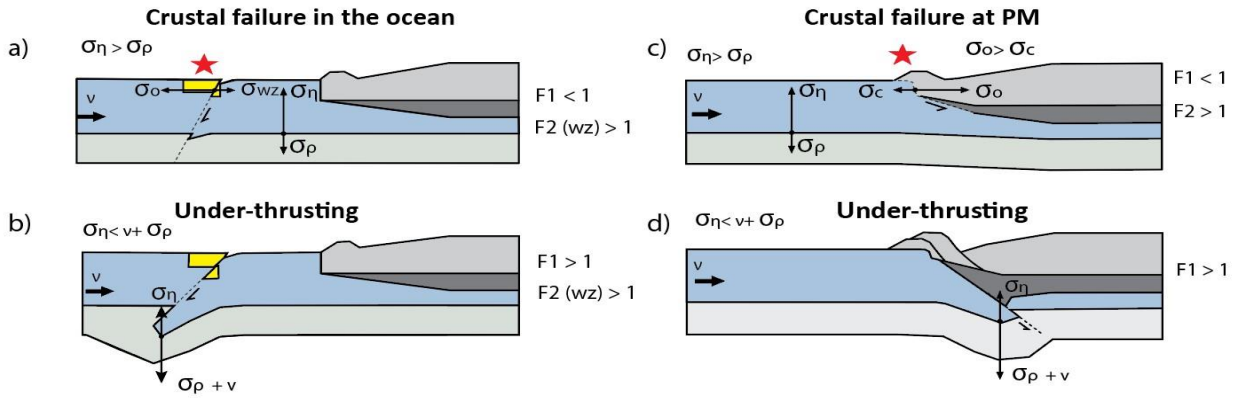

Figure 4.1 Schematic representation of the equilibrium of forces acting in the oceanic domain under compression in the presence and in absence of a weak zone. a) F1 and F2 (wz) are the conditions needed conditions for failure of the crust in the oceanic domain. b) F1 and F2 (wz) are the conditions for subduction initiation. In c) and d) F1 and F2 are the conditions needed for failure at the passive margin and for subduction initiation ath the PM respectively. σρ, ση, σo and σwz is the gravitational force, the viscous mantle resistance force, the oceanic lithosphere strength and the lithospheric strength at the weak zone respectively

controlled by the strength contrast in the lithosphere (Calignano et al., 2015).The oceanic domain must be stronger than the continental one to be able to deform it therefore, the following condition must be fulfilled: F2>1 (Figure 4.1 c) (Auzemery et al. 2019, in revision). Additionally, for subduction initiation the sum of the vertical forces should be able to overcome the viscous resistance of the mantle so the buoyancy number F1 must be >1 (Faccenna et al., 1999). If these 2 conditions are present, deformation localizes at the OCB and subduction zone starts to evolve at the PM (Figure 4.1 c and d). In the weak zone models the initial rheological state is not favourable for intra-oceanic subduction to initiate. F1<1 renders the oceanic domain not buoyant enough to overcome the viscous resistance of the ductile mantle and an F2>1 at the PM prevents deformation to localize initially at the oceanic domain. As such deformation starts always at the passive margin and propagates to the weak zone.

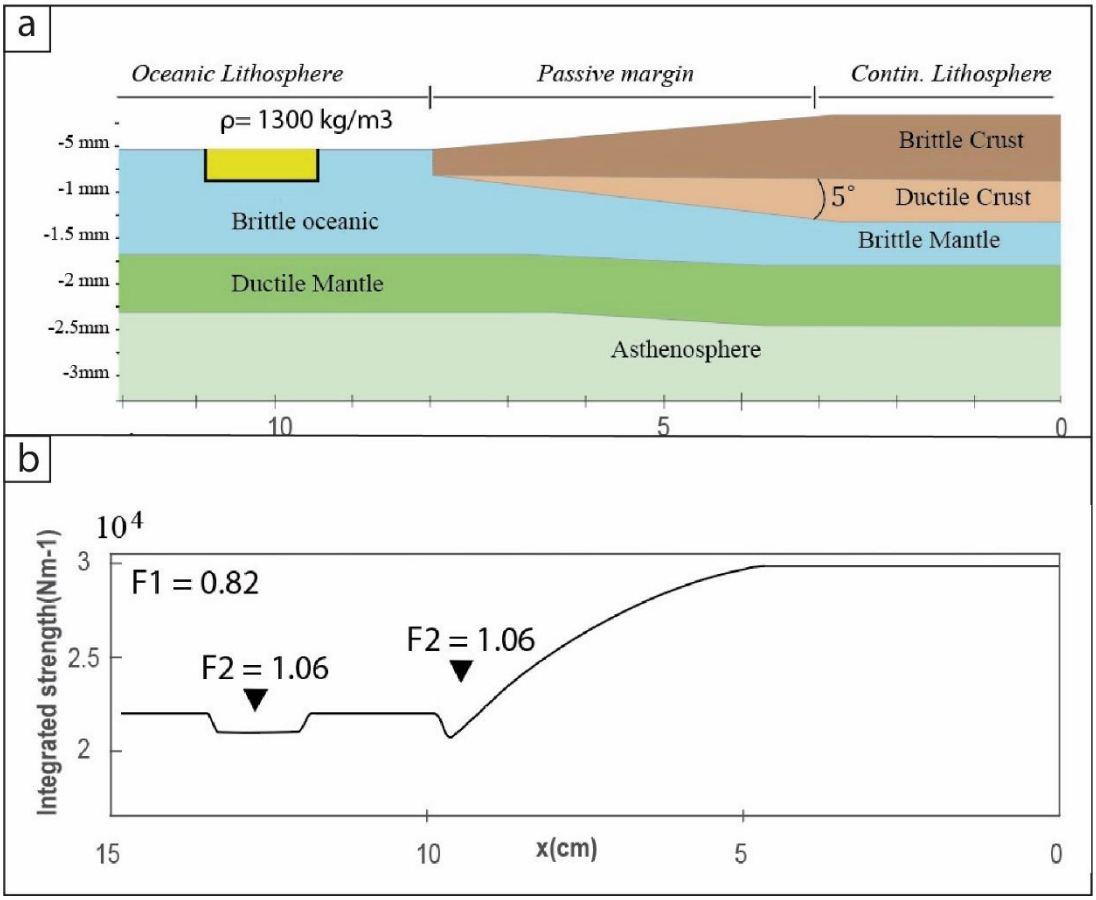

Figure 4.2 a) Graphic representation of the initial rheological model for intermediate oceanic lithosphere and a weak zone in the oceanic domain. b) F1 and F2 ratios along the model

The presence of the weak zone introduces a secondary weakness in the system (Figure 4.2). As the passive margin deforms and increases in thickness, F2 decreases. When F2 at the passive margin becomes smaller than at the weak zone, the weak zone activates and leads to strain localization in oceanic domain. Despite that F1<1 and F2>1, subduction initiates at the oceanic domain and not at the passive margin as it is predicted (Auzemery et al. 2019, in revision) . Therefore, the weak zone plays an important role for localizing deformation and facilitating the deflection of the brittle oceanic lithosphere. The deflection of the lithosphere drives the convergence rate to obtain gradually a vertical component and add up to the vertical force equilibrium changing in this way the buoyancy state of the oceanic lithosphere (F1>1) (Figure 4.2b). In this light, intra-oceanic subduction initiation is possible in the presence of a weak zone even if the initial buoyancy of the oceanic lithosphere is not favouring the initiation of subduction, while numerical models suggest that a density contrast between subcontinental and oceanic ductile lithosphere is needed to initiate subduction (Nikolaeva et al., 2010).

4.1 Intra-oceanic subduction initiation

The topographic evolution along with the final internal structure of the models in this study provide insight in the processes that lead to intra-oceanic subduction.

4.1.1 Crustal deformation and strain localisation

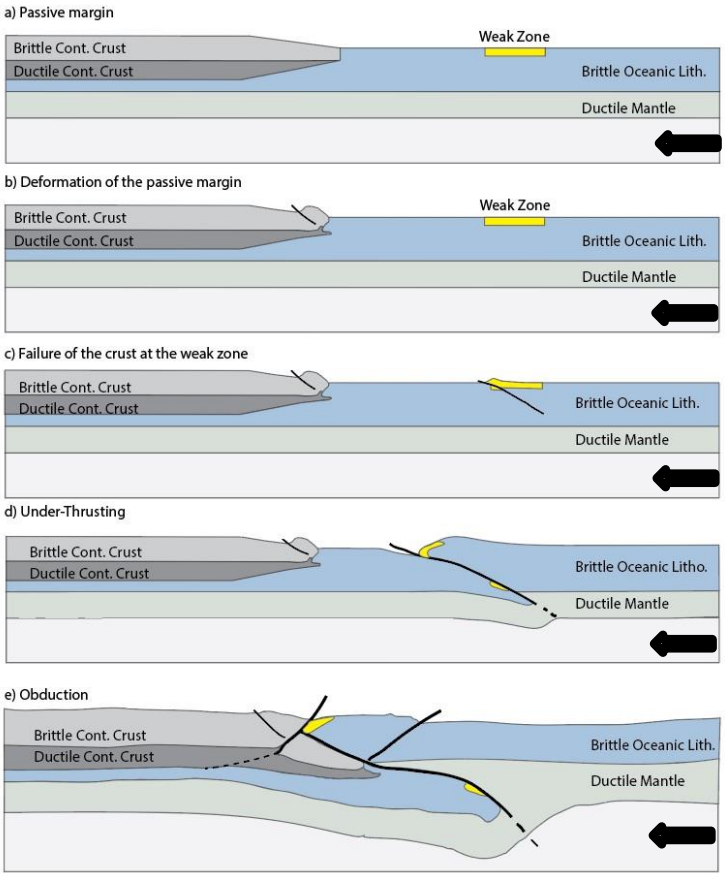

Figure 4.3 a) Representation the initial state of a lithosphere under compression where no deformation has yet occured. b-e) 4 recognised stages of the evolution of intra-oceanic subduction

As suggested in a previous study (Auzemery et al. 2019, in revision) for subduction initiation, except of the wedging out of the ductile continental crust, the rheology of mantle lithosphere is a critical parameter which influences the location of subduction initiation. As it is predicted, at the first stage the deformation is focused on the ocean-continent boundary. This deformation is expressed by shortening of the brittle continental crust accommodated by small fore-thrusts, and ductile deformation of the wedge-shaped ductile continental crust (Figure 4.3b). The first stage is in agreement with other studies on the strain localisation that emphasise the significance of strength contrast within the lithosphere (Calignano et al., 2015; Davy & Cobbold, 1991). In the initial stage, the location of deformation. As it has been shown (Auzemery et al. 2019, in revision), a stronger ocean creates a lateral strength contrast at the passive margin and is able to localise deformation at the OCT. The deformation at the passive margin lasts longer for the experiments with a strong oceanic lithosphere and creates a strong uplift at a wide deformation zone along the OCT while it is brief for a weaker oceanic domain. The second stage of deformation is characterised by the transfer of deformation from the OCT to the weak zone, where the strength contrast (F2) is now the highest. As shortening continues, all the models respond by failure of the ocean crust at this exact location (Figure 4.3c). However, in a weak oceanic lithosphere the amount of shortening at the passive margin is small and deformation quickly transfers to the weak zone.

Conversely, in the case of a strong oceanic lithosphere, the passive margin is deforming continuously until 17% of BS until the rupture of the oceanic crust (Figure 3.3 Exp 2.3). Intra-oceanic strain localisation is probable to occur when the coupling between crust and mantle is weak and the crust and the brittle lithosphere are not strong enough to deform the margin and the flexure of the ductile mantle is insufficient to compensate for the negative buoyancy of the oceanic lithosphere (Auzemery et al. 2019, in revision). However, these experiments show that intra-oceanic strain localisation is feasible with a moderate ductile lithospheric strength and a shallow weak zone o

At and close to the surface of the oceanic crust. The presence of this weak zone reduces the overall lithospheric strength in that location and allows for failure of the crust in the oceanic domain.

4.1.2 Under-thrusting

Under-thrusting of the oceanic lithosphere follows the failure of the crust (Figure 4.3d) and occurs at the boundary of the weak zone. The polarity of the thrust zone is variable, probably controlled by small scale heterogeneities in the model. An intra-oceanic subduction zone forms at the location of the weak zone regardless the strength of surrounding oceanic lithosphere. Although strength of the oceanic lithosphere does not affect the location of under-thrusting, it influences a subsequent polarity change of the thrust. In a weak and moderate strength lithosphere the thrust maintains its polarity but in a strong lithosphere the evolving subduction zone polarity reverses. In this lithospheric configuration, high overall strength of the brittle layers perhaps with the support of the shear resistance of the ductile mantle prevents the thrust to propagate in a similar way to a weak or moderate lithosphere.

The buoyancy forces, described by the buoyancy number F1, acting on the brittle-ductile transition are a factor that can allow or prevent subduction to initiate. As several studies have shown, the formation of a slab requires a negatively buoyant oceanic lithosphere which needs to overcome the resistance of the ductile mantle (McKenzie, 1977; Mueller & Phillips, 1991; K. Nikolaeva et al., 2010). Under conditions where the buoyancy of the lithosphere is slightly insufficient to overcome the shear resistance of the ductile mantle, other processes like the deflection of the lithosphere become important and aid the development of a subduction zone (Figure 4.1b). As for under-thrusting at passive margins, under-thrusting inside the oceanic lithosphere requires then the deformation of the crust and deflection of the lithosphere. If these conditions are not achieved, the lithosphere is supported by its lithospheric mantle, convergence stress remain horizontal and are transferred to the passive margin.

4.1.3 Obduction

The last stage of intra-oceanic subduction leads to the obduction of the overriding plate when it reaches the passive margin (Figure 4.3e). In this model the polarity of the subduction zone is important for obduction to occur. It is important to notice here that in this study we control the localisation of subduction and not the polarity as we do not choose a preferable geometry at the weak zone to control the polarity of the evolving subduction zone. Obduction occurs at the end of the model evolution. Strong deformation of the brittle continental lithosphere by the thick and strong oceanic brittle lithosphere prevents large-scale obduction of oceanic crust on the continent. The analogue modelling technique does not provide a thermal gradient therefore thermal effects, especially at the thrust interface, do not reduce the frictional resistance as it is occurring at natural fault surfaces. This could be another important parameter that prevents obduction to evolve further (Duretz, 2016).

It is, therefore suggested that a heterogeneity located in the oceanic crust domain, is enough to localise deformation. We implement a weakness that it can represent the existence of a zone of serpentinized mantle rocks of a former intra-oceanic core complex and we demonstrate that a small heterogeneity can control strain localisation especially if the forcing is from the mid-ocean ridge continent-ward. This is in agreement with numerical experiments of Maffione, et al. (2015).

4.2 Implication for the Mid-Jurassic Greek and Albanian ophiolites

The Hellenides and the Dinarides offer a good opportunity to study tectonic processes in context of the closure of Neo-Tethys ocean in Late-Jurassic Early-Cretaceous period. The emplacement of ophiolites over continental units such as the Pelagonian passive margin demands the activation of intra-oceanic subduction zones, the successive obduction and finally collision and subduction of Pelagonia under Rhodopia during that times {e.g. Spray et al., 1984; Schermer et al., 1990; Ricou et al., 1998; Sharp & Robertson, 2006). Exhumed low to high grade metamorphic rocks show that the intra-oceanic subduction was followed by obduction of oceanic units over the Pelagonian passive margin {e.g. Schmid et al., 2008; 106 Tomljenović et al., 2008; Kilias et al., 2010). These observations conform with numerical modelling attempts showing that ophiolitic obduction is a stable process in a wide range of physical parameters (Duretz et al., 2016). Intra-oceanic subduction initiation in numerical models suggest that weaknesses in the oceanic domain like detachment faults associated with oceanic core complexes near slow spreading oceanic ridges can localise the deformation causing inversion and subsequently subduction initiation (Maffione et al., 2015). These models require the subduction zone to be only a few tens of kilometres away of the spreading ridge even though the oceanic lithosphere is too young and consequently not buoyant enough to sink into the mantle. Ages of the ophiolitic massifs in Albania and

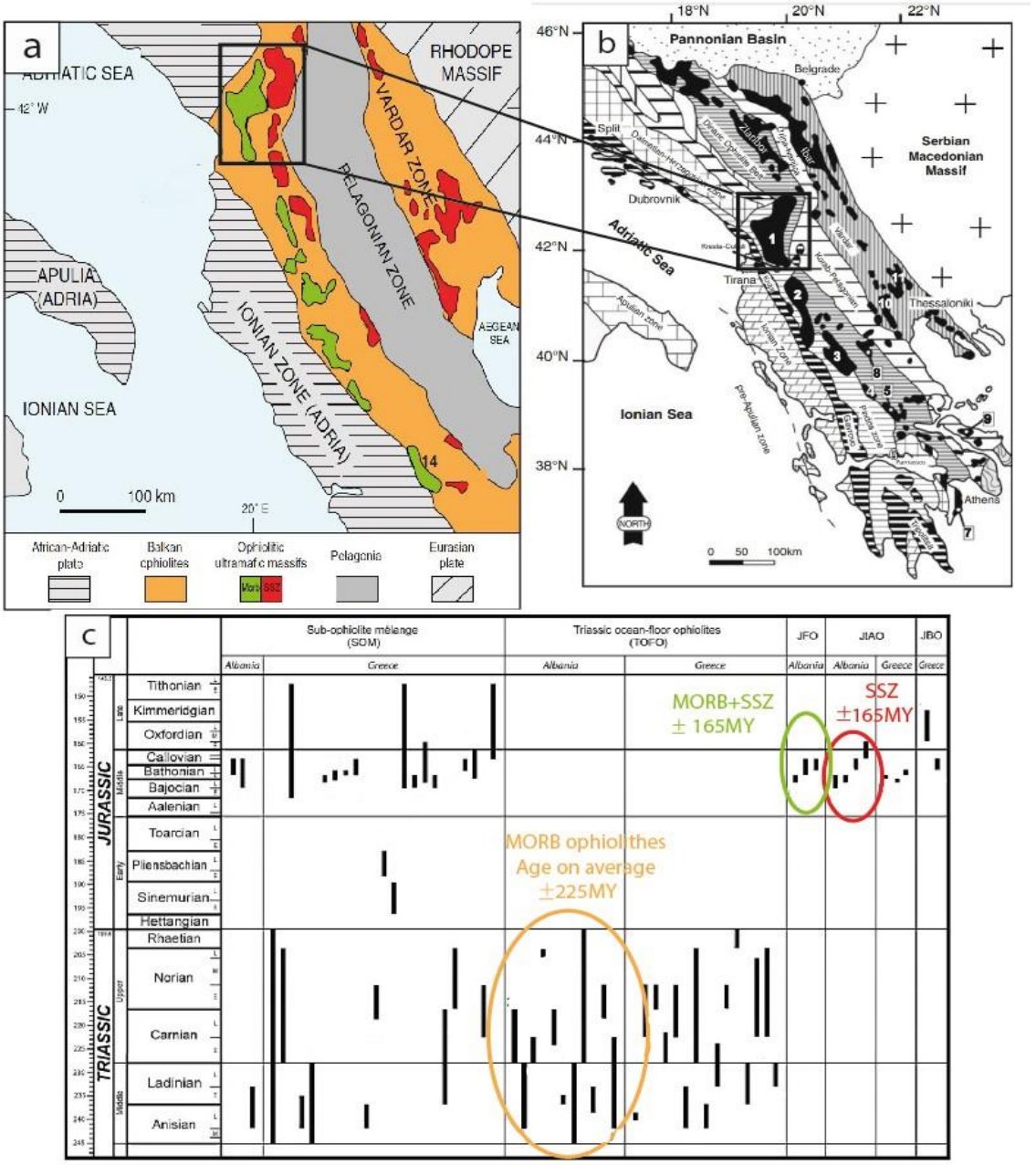

Figure 4.4 a)Simplified regional geological map of central-west Balkan peninsula illustrating the main geological units and the Jurassic ophiolitic belts (Maffione et al., 2015). b) Illustrates the location of the main ophiolitic massifs (solid black). Legend. 1. Mirdita; 2. South Albania; 3. Pindos; 4. Koziakas, 5. Othris; 6. Etolia; 7. Argolis; 8. Vourinos; 9. Evvoia; 10. Almopias; and 11. Guevgueli (Bortolotti et al., 2013). C) A table of the recorded ages of the ophiolitic units. In the coloured circles are the ophiolitic groups of the Mirtida ofiolites and the colour of the circles correspond to the ultramafic massifs that are located in the squered area of figure 4.4a (Bortolotti et al., 2013)

in Greece in Figure 4.4*c* (Bortolotti 2013) show a significant difference between the Triassic Oceanic Floor Ophiolites (TOFO) which have an approximate age of 225My with the Jurassic Fore-arc Ophiolites

(JFO) and the Jurassic intra-oceanic-arc (JIAO) ophiolite with an approximate age of 165My Figure 4.4*c*. According to Bortolotti (2013), JFO consist of a mix of MOR type basalts with SSZ type intrusive sequences interlayered with each other whereas JIAO display only Supra-subduction zone ophiolites. From the analogue models in this study, it can be shown that the initiation of subduction at the location of a pre-existing weaknesses, such as an oceanic core complex or a fracture zone, can be feasible even if the oceanic lithosphere has obtained an intermediate overall strength and thickness. Therefore, intra-oceanic subduction is possible to initiate not a few tens of kilometres away of a slow spreading ridge (Maffione et al., 2015; van Hinsbergen et al., 2016) but a few hundreds. A crustal level weakness in an intermediate oceanic lithosphere is sufficient for the nucleation of deformation that is required for intra-oceanic subduction initiation. Hereby, an evolutionary model is proposed that can explain regional scale tectonic events such as the closure and obduction of Neo-Tethyan ocean over the Pelagonian passive margin in Jurassic – Early Cretaceous times.

In this study the model that is proposed for the closure of an ocean that existed in middle Triassic to Middle Jurassic times is based on the analytical records of the ophiolitic unites and the associated stratigraphic data from the ophiolitic zones in Greece and Albania (Bortolotti 2013) and the proposal of a single oceanic basin during Triassic between Adria and Eurasia passive margins. {Bernulli and Laubscher 1972). Figure 4.5 illustrates the succession of evolutional stages from Late Triassic to Early Cretaceous times. After continuous spreading of the ocean during Triassic and until Early Jurassic it has been estimated that the ocean floor obtained a width of 1200km in about 70My (Bortolotti and refs in there). In this slow spreading rates of 1-2cm/yr and according to observed and mapped ancient Oceanic Core Complexes in Mirdita ophiolites (Maffione et al., 2013) the occurrence of detachment faults near the mid-oceanic ridge (Figure 4.5a) led to serpentinisation of the exhumed mantle rocks and consequently to the formation of weak zones within the oceanic crust during Middle – Late Triassic. The spreading of the oceanic floor continued and Early Jurassic (185Ma) compressional forces start to apply (Bortolotti 2013) leading to failure of the oceanic crust by inverting the pre-existing detachment faults (Figure 4.5b). This stage is closely related with the first evolutional stage as it has been described in Figure 4.3c, inferred from the experimental results mainly from experiment 2.2 (Figure 3.3b). Approximately 20My later, corresponding to the under-thrusting and subduction stage (Figure 4.3d), the ophiolitic unit of JFO start to form (Figure 4.5c). The co-existence of SSZ-type sequences into the Middle-Jurassic MORB-type sequences (Bortolotti 2013) indicates that the subducting slab reached a depth that allows the production and ascension of melt to the oceanic ridge. The emplacement of the JFO unit west of the JIAO unit is a direct indication that the subduction zone is located in the oceanic

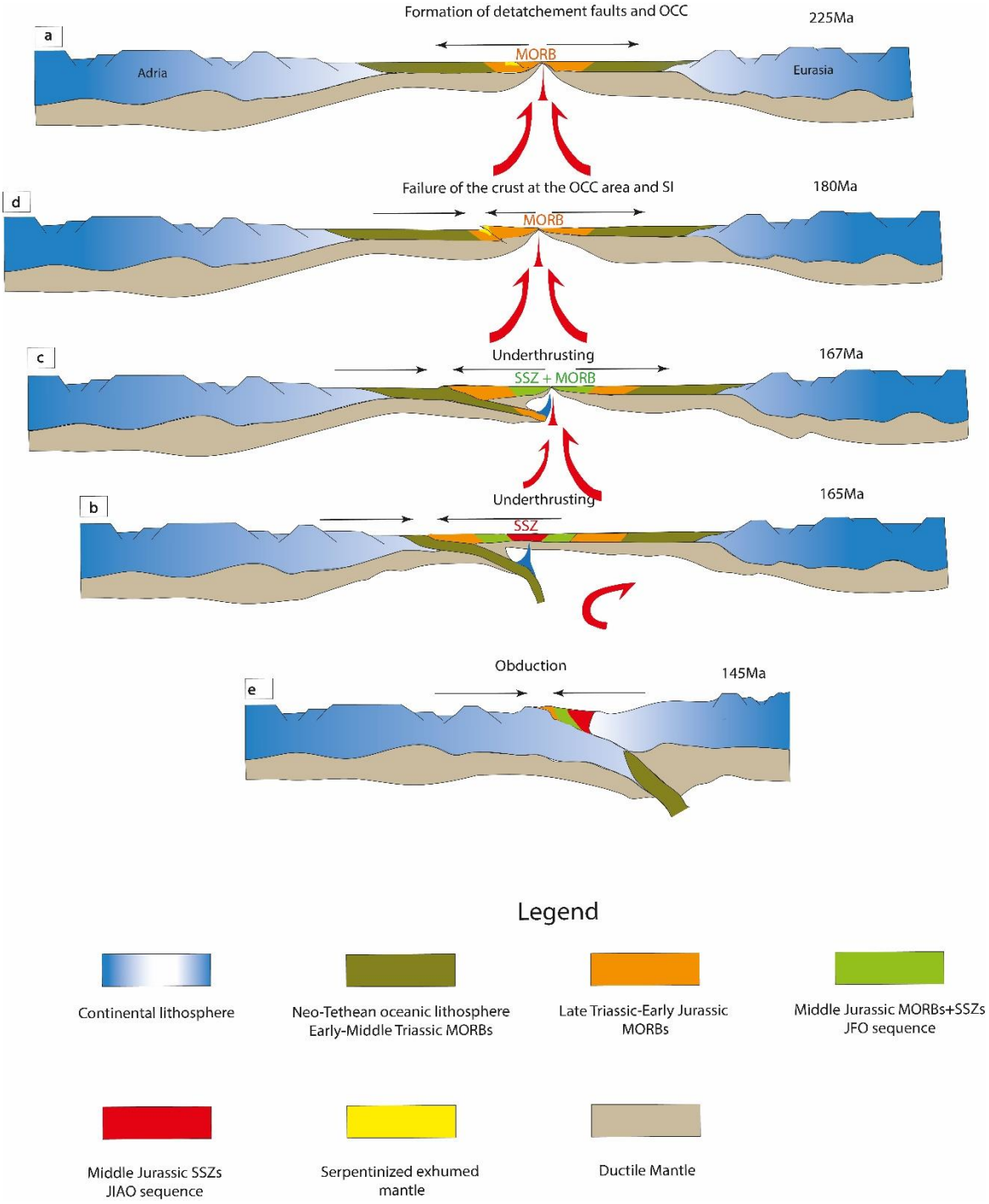

Figure 4.5 A 2-dimentional, simplified and not to scale illustration of the tectonic evolution of a Triassic ocean occurred between Andria and Eurasia continental block from the Mid-Jurassic subduction initiation until the Early Cretaceous obduction on Andria's passive margin. This representation describes all the stages of Intra-oceanic Subduction Initiation that describes earlier, from failure of the crust at the weak zone to the last stage of obduction (4.1.3).

domain connected to Adria continent and it is dipping towards Eurasia. In a later stage (Figure 4.5d) which took place a few million years later according to the table in Figure 4.5c, the JIAO unit consists of

SSZ intrusive sequences. Absence of MORB type volcanism in JIAO highlights the cease of activity of the mid-oceanic ridge in Middle Jurassic (165Ma). In agreement with the model results of this study and the stage of obduction (Figure 4.3e), at the final stage the subduction continues consuming the oceanic floor and leading to the obduction of the propagating lithosphere above the Adria's passive margin Figure 4.5e) in Late Cretaceous (145Ma).

5 CONCLUSIONS

In this study, analogue experiments have been conducted with the main objective to gain insight into the role of pre-existing weakness in the oceanic domain in context of intra-oceanic subduction. The simulated lithospheres incorporate an oceanic and a continental domain separated by a wedge-shaped continental margin. A weak zone has been implemented in the oceanic crust to represent natural strength heterogeneities such as an oceanic core complex or fracture zones. The deformation in the models has been assumed to be caused by far-field forces.

According to the model results the following points can be highlighted:

1. The weak zone plays a substantial role for localising deformation. This effect is when the bulk strength of the oceanic plate is low or intermediate. In cases of an overall high strength oceanic lithosphere, deformation predominantly takes place at the OCT. It creates rheological heterogeneities in the oceanic lithosphere allowing formation of a deformation zone after a brief deformational episode at the passive margin.
2. Intra-oceanic subduction initiation is evolving in the following successive stages: a) deformation of the passive margin, b) failure of the crust at the weak zone, c) under-thrusting and subduction followed by obduction of oceanic crust.
3. At the under-thrusting stage, subduction slabs with a low subduction angle form in a weak/medium strength oceanic lithosphere, whereas with a strong profile the subduction zone changes polarity quickly forming a pop-down structure.
4. Obduction is possible for ocean-ward dipping subduction .

Conclusively, despite the difficulty for oceanic plate to fail under compression, the existence of a crustal level weak zone (i.e. former oceanic core complexes) can localise strain and trigger subduction initiation in the intra-oceanic domain. This is in accordance with subduction initiation processes responsible for the closure of the Neo-Tethys ocean where intra-oceanic subduction initiation at a core complex is documented.

6 REFERENCES

Alvarez-Marron, J., E. Rubio & M. Torn (1997) Subduction-related structures in the North Iberian margin. *Journal of Geophysical Research: Solid Earth***,** 22497-22511.

Andreani, M., J. Escartin, A. Delacour, B. Ildefonse, M. Godard, J. Dyment, A. E. Fallick & Y. Fouquet (2014) Tectonic structure, lithology, and hydrothermal signature of the Rainbow massif (Mid-Atlantic Ridge 36° 14′ N). *Geochemistry, Geophysics, Geosystems,* 15**,** 3543-3571.

Assumpção, M. (1998) Seismicity and stresses in the Brazilian passive margin. *Bulletin of the Seismological Society of America,* 88**,** 160-169.

A. Auzemery1, D. Sokoutis1,2, E. Willingshofer1, J. P. Brun3 (2019) Subduction initiation at passive margins, inferences from analogue modelling, *in revision*

Bach, W., C. J. Garrido, H. Paulick, J. Harvey & M. Rosner (2004) Seawater-peridotite interactions: First insights from ODP Leg 209, MAR 15 N. *Geochemistry, Geophysics, Geosystems,* 5.

Bach, W., H. Paulick, C. J. Garrido, B. Ildefonse, W. P. Meurer & S. E. Humphris (2006) Unraveling the sequence of serpentinization reactions: petrography, mineral chemistry, and petrophysics of serpentinites from MAR 15 N (ODP Leg 209, Site 1274). *Geophysical research letters,* 33.

Bayrakci, G., T. Minshull, D. Sawyer, T. J. Reston, D. Klaeschen, C. Papenberg, C. Ranero, J. Bull, R. Davy & D. Shillington (2016) Fault-controlled hydration of the upper mantle during continental rifting. *Nature Geoscience,* 9**,** 384.

Beard, J. S., B. R. Frost, P. Fryer, A. McCaig, R. Searle, B. Ildefonse, P. Zinin & S. K. Sharma (2009) Onset and progression of serpentinization and magnetite formation in olivine-rich troctolite from IODP Hole U1309D. *Journal of Petrology,* 50**,** 387-403.

Bernoulli, D. (1972) The palinspastic problem of the Hellenides. *Eclogae Geologicae Helvetiae,* 65**,** 107-118.

Billen, M. I. & G. Hirth (2005) Newtonian versus non-Newtonian upper mantle viscosity: Implications for subduction initiation. *Geophysical Research Letters,* 32.

Bills, B. G., D. R. Currey & G. A. Marshall (1994) Viscosity estimates for the crust and upper mantle from patterns of lacustrine shoreline deformation in the Eastern Great Basin. *Journal of Geophysical Research: Solid Earth,* 99**,** 22059-22086.

Bortolotti, V., M. Chiari, M. Marroni, L. Pandolfi, G. Principi & E. Saccani (2013) Geodynamic evolution of ophiolites from Albania and Greece (Dinaric-Hellenic belt): one, two, or more oceanic basins? *International Journal of Earth Sciences,* 102**,** 783-811.

Boschi, C., E. Bonatti, M. Ligi, D. Brunelli, A. Cipriani, L. Dallai, M. D'Orazio, G. L. Früh-Green, S. Tonarini & J. D. Barnes (2013) Serpentinization of mantle peridotites along an uplifted lithospheric section, Mid Atlantic Ridge at 11 N. *Lithos,* 178**,** 3-23.

Boschi, C., G. L. Früh-Green, A. Delacour, J. A. Karson & D. S. Kelley (2006) Mass transfer and fluid flow during detachment faulting and development of an oceanic core complex, Atlantis Massif (MAR 30 N). *Geochemistry, Geophysics, Geosystems,* 7.

Brace, W. & D. Kohlstedt (1980) Limits on lithospheric stress imposed by laboratory experiments. *Journal of Geophysical Research: Solid Earth,* 85**,** 6248-6252.

Brun, J.-P. (2002) Deformation of the continental lithosphere: Insights from brittle-ductile models. *Geological Society, London, Special Publications,* 200**,** 355-370.

Buck, W. R. (1991) Modes of continental lithospheric extension. *Journal of Geophysical Research,* 96**,** 20161-20178.

Burov, E. B. (2011) Rheology and strength of the lithosphere. *Marine and Petroleum Geology,* 28**,** 1402-1443.

Burov, E. B. & M. Diament (1995) The effective elastic thickness (Te) of continental lithosphere: What does it really mean? *Journal of Geophysical Research,* 100**,** 3905-3927.

Byerlee, J. 1978. Friction of rocks. In *Rock friction and earthquake prediction*, 615-626. Springer.

Cann, J., D. Blackman, D. Smith, E. McAllister, B. Janssen, S. Mello, E. Avgerinos, A. Pascoe & J. Escartin (1997) Corrugated slip surfaces formed at ridge–transform intersections on the Mid-Atlantic Ridge. *Nature,* 385**,** 329.

Calignano, E., D. Sokoutis, E. Willingshofer, J. P. Brun, F. Gueydan & S. Cloetingh (2017) Oblique contractional reactivation of inherited heterogeneities: Cause for arcuate orogens. *Tectonics,* 36**,** 542-558.

Calignano, E., D. Sokoutis, E. Willingshofer, F. Gueydan & S. Cloetingh (2015) Strain localization at the margins of strong lithospheric domains: Insights from analog models. *Tectonics,* 34**,** 396-412.

Casey, J. F. & J. F. Dewey (1984) Initiation of subduction zones along transform and accreting plate boundaries, triple-junction evolution, and forearc spreading centres—implications for ophiolitic geology and obduction. *Geological Society, London, Special Publications,* 13**,** 269-290.

Cloetingh, S., M. J. R. Wortel & N. J. Vlaar (1982) Evolution of passive continental margins and initiation of subduction zones. *Nature,* 297**,** 139-142.

Cloetingh, S., R. Wortel & N. Vlaar. 1989. On the initiation of subduction zones. In *Subduction Zones Part II*, 7-25. Springer.

Contrucci, I., L. Matias, M. Moulin, L. Géli, F. Klingelhöfer, H. Nouzé, D. Aslanian, J.-L. Olivet, J.-P. Réhault & J.-C. Sibuet (2004) Deep structure of the West African continental margin (Congo, Zaïre, Angola), between 5°S and 8°S, from reflection/refraction seismics and gravity data. *Geophysical Journal International,* 158**,** 529-553.

Davy, P. & P. Cobbold (1991) Experiments on shortening of a 4-layer model of the continental lithosphere. *Tectonophysics,* 188**,** 1-25.

DeMets, C., R. G. Gordon & D. F. Argus (2010) Geologically current plate motions. *Geophysical Journal International,* 181**,** 1-80.

Dewey, J. F. & J. M. Bird (1970) Mountain Belts and the New Global Tectonics. *Journal of Geophysical Research,* 75**,** 2625–2647.

Dick, H. J., J. Lin & H. Schouten (2003) An ultraslow-spreading class of ocean ridge. *Nature,* 426**,** 405.

Djomani, Y. H. P., S. Y. O'Reilly, W. L. Griffin, W. L. Griffin & P. E. D. Morgan (2001) The density

structure of subcontinental lithosphere through time. *Earth and Planetary Science Letters,* 184**,** 605-621.

Drury, M. (2005) Dynamic recrystallization and strain softening of olivine aggregates in the laboratory and the lithosphere. *Geological Society, London, Special Publications***,** 143-158.

Duretz, T., P. Agard, P. Yamato, C. Ducassou, E. B. Burov & T. V. Gerya (2016) Thermo-mechanical modeling of the obduction process based on the Oman ophiolite case. *Gondwana Research,* 32**,** 1-10.

England, P. & R. Wortel (1980) Some consequences of the subduction of young slabs. *Earth and Planetary Science Letters,* 47**,** 403-415.

Escartin, J., G. Hirth & B. Evans (1997) Nondilatant brittle deformation of serpentinites: Implications for Mohr-Coulomb theory and the strength of faults. *Journal of Geophysical Research: Solid Earth,* 102**,** 2897-2913.

Escartin, J., (2001) Strength of slightly serpentinized peridotites: Implications for the tectonics of oceanic lithosphere. *Geology,* 29**,** 1023-1026.

Escartín, J., C. Mével, C. J. MacLeod & A. McCaig (2003) Constraints on deformation conditions and the origin of oceanic detachments: The Mid-Atlantic Ridge core complex at 15 45′ N. *Geochemistry, Geophysics, Geosystems,* 4.

Escartín, J., D. K. Smith, J. Cann, H. Schouten, C. H. Langmuir & S. Escrig (2008) Central role of detachment faults in accretion of slow-spreading oceanic lithosphere. *Nature,* 455**,** 790.

Faccenda, M., L. Burlini, T. V. Gerya & D. Mainprice (2008) Fault-induced seismic anisotropy by hydration in subducting oceanic plates. *Nature,* 455**,** 1097-1100.

Faccenna, C., D. Giardini, P. Davy & A. Argentieri (1999) Initiation of subduction at Atlantic-type margins: Insights from laboratory experiments. *Journal of Geophysical Research: Solid Earth***,** 2749-2766.

Fox, P. J. & D. G. Gallo (1984) A tectonic model for ridge-transform-ridge plate boundaries: Implications for the structure of oceanic lithosphere. *Tectonophysics,* 104**,** 205-242.

Garcees, M. & J. S. Gee (2007) Paleomagnetic evidence of large footwall rotations associated with low-angle faults at the Mid-Atlantic Ridge. *Geology***,** 279-282.

Gerya, T. V., J. A. D. Connolly & D. A. Yuen (2008) Why is terrestrial subduction one-sided? *Geology,* 36**,** 43-46.

Goren, L., E. Aharonov, G. Mulugeta, H. Koyi, Y. Mart & Y. Mart (2008) Ductile deformation of passive margins: A new mechanism for subduction initiation. *Journal of Geophysical Research,* 113.

Grevemeyer, I., N. W. Hayman, C. Peirce, M. Schwardt, H. J. Van Avendonk, A. Dannowski & C. Papenberg (2018) Episodic magmatism and serpentinized mantle exhumation at an ultraslow-spreading centre. *Nature Geoscience,* 11**,** 444.

Guillot, S., S. Schwartz, B. Reynard, P. Agard & C. Prigent (2015) Tectonic significance of serpentinites. *Tectonophysics,* 646**,** 1-19.

Gurnis, M., C. Hall & L. Lavier (2004) Evolving force balance during incipient subduction. *Geochemistry, Geophysics, Geosystems,* 5.

Gülcher, A. J., S. J. Beaussier & T. V. Gerya (2019) On the formation of oceanic detachment faults

and their influence on intra-oceanic subduction initiation: 3D thermomechanical modeling. *Earth and Planetary Science Letters,* 506**,** 195-208.

Hall, C. E., M. Gurnis, M. Sdrolias, L. L. Lavier & R. D. Müller (2003) Catastrophic initiation of subduction following forced convergence across fracture zones. *Earth and Planetary Science Letters,* 212**,** 15-30.

Hawkins, J. W., S. H. Bloomer, C. A. Evans & J. T. Melchior (1984) Evolution of intra-oceanic arc-trench systems. *Tectonophysics,* 102**,** 175-205.

Hirth, G. & D. Kohlstedt (2003) Rheology of the upper mantle and the mantle wedge: A view from the experimentalists. *Inside the subduction Factory***,** 83-105.

Jaeger, J. & N. GoW (1979) Cook. *NGW Fundamentals of Rock Mechanics 3rd edn London: Chapman and Hall*.

Jolivet, L., C. Faccenna, B. Huet, L. Labrousse, L. Le Pourhiet, O. Lacombe, E. Lecomte, E. Burov, Y. Denele, J.-P. Brun & others (2013) Aegean tectonics: Strain localisation, slab tearing and trench retreat. *Tectonophysics***,** 1-13.

Karig, D. E. (1982) Initiation of subduction zones: implications for arc evolution and ophiolite development. *Geological Society, London, Special Publications,* 10**,** 563-576.

Kaufmann, G. & F. Amelung (2000) Reservoir-induced deformation and continental rheology in vicinity of Lake Mead, Nevada (Paper 2000JB900079). *JOURNAL OF GEOPHYSICAL RESEARCH-ALL SERIES-,* 105**,** 16,341-16,358.

Kilias, A., W. Frisch, A. Avgerinas, I. Dunkl, G. Falalakis & H.-J. Gawlick (2010) Alpine architecture and kinematics of deformation of the northern Pelagonian nappe pile in the Hellenides. *Austrian Journal of Earth Sciences,* 103**,** 4-28.

Kirby, S. H. (1985) Rock mechanics observations pertinent to the rheology of the continental lithosphere and the localization of strain along shear zones. *Tectonophysics,* 119**,** 1-27.

Klein, F., W. Bach, N. Jöns, T. McCollom, B. Moskowitz & T. Berquó (2009) Iron partitioning and hydrogen generation during serpentinization of abyssal peridotites from 15 N on the Mid-Atlantic Ridge. *Geochimica et Cosmochimica Acta,* 73**,** 6868-6893.

Korenaga, T. & J. Korenaga (2016) Evolution of young oceanic lithosphere and the meaning of seafloor subsidence rate. *Journal of Geophysical Research: Solid Earth***,** 6315-6332.

Kusznir, N. J. & R. G. Park (1984) Intraplate lithosphere deformation and the strength of the lithosphere. *Geophysical Journal International,* 79**,** 513-538.

Lambeck, K., C. Smither & P. Johnston (1998) Sea-level change, glacial rebound and mantle viscosity for northern Europe. *Geophysical Journal International,* 134**,** 102-144.

Leat, P. & R. Larter (2003) Intra-oceanic subduction systems: introduction. *Geological Society, London, Special Publications,* 219**,** 1-17.

MacLeod, C., R. Searle, B. Murton, J. Casey, C. Mallows, S. Unsworth, K. Achenbach & M. Harris (2009) Life cycle of oceanic core complexes. *Earth and Planetary Science Letters,* 287**,** 333-344.

MacLeod, C. J., J. Carlut, J. Escartín, H. Horen & A. Morris (2011) Quantitative constraint on footwall rotations at the 15° 45′ N oceanic core complex, Mid-Atlantic Ridge: Implications for oceanic detachment fault processes. *Geochemistry, Geophysics, Geosystems,* 12.

MacLeod, C. J., J. Escartin, D. Banerji, G. Banks, M. Gleeson, D. H. B. Irving, R. Lilly, A. McCaig, Y. Niu & S. Allerton (2002) Direct geological evidence for oceanic detachment faulting: The Mid-Atlantic Ridge, 15 45′ N. *Geology,* 30**,** 879-882.

Marco Maffione, Antony Morris & Mark W. Anderson (2013) Recognizing detachment-mode seafloor spreading in the deep geological past. SCIENTIFIC REPORTS | 3 : 2336 | DOI: 10.1038/srep02336

Maffione, M., A. Morris, O. Plümper & D. J. van Hinsbergen (2014) Magnetic properties of variably serpentinized peridotites and their implication for the evolution of oceanic core complexes. *Geochemistry, Geophysics, Geosystems,* 15**,** 923-944.

Maffione, M., C. Thieulot, D. J. J. van Hinsbergen, A. Morris, O. Plümper & W. Spakman (2015) Dynamics of intraoceanic subduction initiation: 1. Oceanic detachment fault inversion and the formationof supra-subduction zone ophiolites. *Geochem. Geophys. Geosyst.***,** 16.

Masson, D., J. Cartwright, L. Pinheiro, R. Whitmarsh, M. O. Beslier & H. Roeser (1994) Compressional deformation at the ocean--continent transition in the NE Atlantic. *Journal of the Geological Society***,** 607-613.

Matsumoto, T. & Y. Tomoda (1983) Numerical simulation of the initiation of subduction at the fracture zone. *Journal of Physics of the Earth***,** 183-194.

Maystrenko, Y., Petrovich & W. Scheck, Magdalena (2013) 3D lithosphere-scale density model of the Central European Basin System and adjacent areas. *Tectonophysics,* 601**,** 53-77.

Maystrenko, Y. & M. Scheck-Wenderoth (2009) Density contrasts in the upper mantle and lower crust across the continent—ocean transition: constraints from 3-D gravity modelling at the Norwegian margin. *Geophysical Journal International,* 179**,** 536-548.

McKenzie, D. P. (1977) The initiation of trenches: a finite amplitude instability. Island arcs, deep sea trenches and back-arc basins. 57-61.

Midtkandal, I., J.-P. Brun, R. H. Gabrielsen & R. S. Huismans (2013) Control of lithosphere rheology on subduction polarity at initiation: Insights from 3D analogue modelling. *Earth and Planetary Science Letters,* 361**,** 219-228.

Mitrovica, J. X. & A. M. Forte (1997) Radial profile of mantle viscosity: results from the joint inversion of convection and postglacial rebound observables. *Journal of Geophysical Research: Solid Earth,* 102**,** 2751-2769.

Mixon, R. B. & W. L. Newell (1977) Stafford fault system: Structures documenting Cretaceous and Tertiary deformation along the Fall Line in northeastern Virginia. *Geology,* 5**,** 437-440.

Morris, A., J. Gee, N. Pressling, B. John, C. J. MacLeod, C. Grimes & R. Searle (2009) Footwall rotation in an oceanic core complex quantified using reoriented Integrated Ocean Drilling Program core samples. *Earth and Planetary Science Letters,* 287**,** 217-228.

Mueller, S. & R. J. Phillips (1991) On The initiation of subduction. *Journal of Geophysical Research,* 96**,** 651-665.

Mével, C. (2003) Serpentinization of abyssal peridotites at mid-ocean ridges. *Comptes Rendus Geoscience,* 335**,** 825-852.

Nalpas, T. & J.-P. Brun (1993) Salt flow and diapirism related to extension at crustal scale. *Tectonophysics,* 228**,** 349-362.

Natland, J. (1981) Petrologic evolution of the Mariana arc and back-arc basin system: a synthesis of drilling results in the south Philippine Sea. *Initial reports of the deep sea drilling project,* 60**,** 877-908.

Nikolaeva, K., T. V. Gerya & J. A. D. Connolly (2008) Numerical modelling of crustal growth in intraoceanic volcanic arcs. *Physics of the Earth and Planetary Interiors,* 171**,** 336-356.

Nikolaeva, K., T. V. Gerya, T. V. Gerya, F. O. Marques & F. O. Marques (2010) Subduction initiation at passive margins: Numerical modeling. *Journal of Geophysical Research,* 115.

Nikolaeva, Ksenia, Gerya, Taras V., Marques, Fernando O. (2011) Numerical analysis of subduction initiation risk along the Atlantic American passive margins. *Geology,* 39**,** 463-466.

Ohara, Y., T. Yoshida, Y. Kato & S. Kasuga (2001) Giant megamullion in the Parece Vela backarc basin. *Marine Geophysical Researches,* 22**,** 47-61.

Osmundsen, P. T. & T. F. Redfield (2011) Crustal taper and topography at passive continental margins. *Terra Nova,* 23**,** 349-361.

Plümper, O., A. Beinlich, W. Bach, E. Janots & H. Austrheim (2014) Garnets within geode-like serpentinite veins: Implications for element transport, hydrogen production and life-supporting environment formation. *Geochimica et Cosmochimica Acta,* 141**,** 454-471.

Plümper, O., A. Røyne, A. Magrasó & B. Jamtveit (2012) The interface-scale mechanism of reaction-induced fracturing during serpentinization. *Geology,* 40**,** 1103-1106.

Ramberg, H. (1981) The role of gravity in orogenic belts. *Geological Society, London, Special Publications,* 9**,** 125-140.

Ranalli, G. 1995. *Rheology of the Earth*. Springer Science & Business Media.

Regenauer-Lieb, K., D. A. Yuen & J. M. Branlund (2001) The Initiation of Subduction: Criticality by Addition of Water? *Science,* 294**,** 578-580.

Reston, T. & C. R. Ranero (2011) The 3-D geometry of detachment faulting at mid-ocean ridges. *Geochemistry, Geophysics, Geosystems,* 12.

Ricou, L.-E., J.-P. Burg, I. Godfriaux & Z. Ivanov (1998) Rhodope and Vardar: the metamorphic and the olistostromic paired belts related to the Cretaceous subduction under Europe. *Geodinamica Acta,* 11**,** 285-309.

Sauter, D., M. Cannat, S. Rouméjon, M. Andreani, D. Birot, A. Bronner, D. Brunelli, J. Carlut, A. Delacour & V. Guyader (2013) Continuous exhumation of mantle-derived rocks at the Southwest Indian Ridge for 11 million years. *Nature Geoscience,* 6**,** 314.

Schellart, W. P. & V. Strak (2016) A review of analogue modelling of geodynamic processes: Approaches, scaling, materials and quantification, with an application to subduction experiments. *Journal of Geodynamics,* 100**,** 7-32.

Schermer, E. R., D. R. Lux & B. C. Burchfiel (1990) Temperature-time history of subducted continental crust, Mount Olympos Region, Greece. *Tectonics,* 9**,** 1165-1195.

Schmid, S. M., D. Bernoulli, B. Fügenschuh, L. Matenco, S. Schefer, R. Schuster, M. Tischler & K. Ustaszewski (2008) The Alpine-Carpathian-Dinaridic orogenic system: correlation and evolution of tectonic units. *Swiss Journal of Geosciences,* 101**,** 139-183.

Schroeder, T., B. John & B. R. Frost (2002) Geologic implications of seawater circulation through peridotite exposed at slow-spreading mid-ocean ridges. *Geology,* 30**,** 367-370.

Sharp, I. R. & A. H. Robertson (2006) Tectonic-sedimentary evolution of the western margin of the Mesozoic Vardar Ocean: evidence from the Pelagonian and Almopias zones, northern Greece. *Geological Society, London, Special Publications,* 260**,** 373-412.

Smit, J., J. Brun & D. Sokoutis (2003) Deformation of brittle-ductile thrust wedges in experiments and nature. *Journal of Geophysical Research: Solid Earth,* 108.

Smith, D. K., J. R. Cann & J. Escartín (2006) Widespread active detachment faulting and core complex formation near 13 N on the Mid-Atlantic Ridge. *Nature,* 442**,** 440.

Smith, D. K., J. Escartín, H. Schouten & J. R. Cann (2008) Fault rotation and core complex formation: Significant processes in seafloor formation at slow-spreading mid-ocean ridges (Mid-Atlantic Ridge, 13–15 N). *Geochemistry, Geophysics, Geosystems,* 9.

Sokoutis, D., J.-P. Burg, M. Bonini, G. Corti & S. Cloetingh (2005) Lithospheric-scale structures from the perspective of analogue continental collision. *Tectonophysics,* 406**,** 1-15.

Solomatov, V. (1995) Scaling of temperature-and stress-dependent viscosity convection. *Physics of Fluids,* 7**,** 266-274.

Solomatov, V. S. (1998) Scaling of temperature- and stress-dependent viscosity convection.

Spray, J., J. Bébien, D. Rex & J. Roddick (1984) Age constraints on the igneous and metamorphic evolution of the Hellenic-Dinaric ophiolites. *Geological Society, London, Special Publications,* 17**,** 619-627.

Stein, S., S. Cloetingh, N. H. Sleep & R. Wortel. 1989. Passive margin earthquakes, stresses and rheology.

Stern, R. J. (2004) Subduction initiation: spontaneous and induced. *Earth and Planetary Science Letters***,** 275 - 292.

Stern, R. J. & S. H. Bloomer (1992) Subduction zone infancy: examples from the Eocene Izu-Bonin-Mariana and Jurassic California arcs. *Geological Society of America Bulletin,* 104**,** 1621-1636.

Stern, R. J. & T. Gerya (2018) Subduction initiation in nature and models: A review. *Tectonophysics,* 746**,** 173-198.

Tomljenović, B., L. Csontos, E. Márton & P. Márton (2008) Tectonic evolution of the northwestern Internal Dinarides as constrained by structures and rotation of Medvednica Mountains, North Croatia. *Geological Society, London, Special Publications,* 298**,** 145-167.

Toth, J. & M. Gurnis (1998) Dynamics of subduction initiation at preexisting fault zones. *Journal of Geophysical Research: Solid Earth,* 103**,** 18053-18067.

Unternehr, P., G. Peron-Pinvidic, G. Manatschal & E. Sutra (2010) Hyper-extended crust in the South Atlantic: in search of a model. *Petroleum Geoscience,* 16**,** 207-215.

van Hinsbergen, D. J., M. Maffione, A. Plunder, N. Kaymakcı, M. Ganerød, B. W. Hendriks, F. Corfu, D. Gürer, G. I. de Gelder & K. Peters (2016) Tectonic evolution and paleogeography of the Kırşehir Block and the Central Anatolian Ophiolites, Turkey. *Tectonics,* 35**,** 983-1014.

van Hunen, J., S. Zhong, N. M. Shapiro & M. H. Ritzwoller (2005) New evidence for dislocation creep from 3-D geodynamic modeling of the Pacific upper mantle structure. *Earth and Planetary Science Letters,* 238**,** 146-155.

Vergnolle, M., F. Pollitz & E. Calais (2003) Constraints on the viscosity of the continental crust and

mantle from GPS measurements and postseismic deformation models in western Mongolia. *Journal of Geophysical Research: Solid Earth,* 108.

Vlaar, N. & M. Wortel (1976) Lithospheric aging, instability and subduction. *Tectonophysics***,** 331-351.

Watts, A. & S. Zhong (2000) Observations of flexure and the rheology of oceanic lithosphere. *Geophysical Journal International,* 142**,** 855-875.

Watts, A. B. & E. Burov (2003) Lithospheric strength and its relationship to the elastic and seismogenic layer thickness. *Earth and Planetary Science Letters,* 213**,** 113-131.

Weertman, J. (1978) Creep laws for the mantle of the Earth. *Philosophical Transactions of the Royal Society of London. Series A, Mathematical and Physical Sciences,* 288**,** 9-26.

Weijermars, R. (1986) Flow behaviour and physical chemistry of bouncing putties and related polymers in view of tectonic laboratory applications. *Tectonophysics,* 124**,** 325-358.

Whitney, D. L., C. Teyssier, P. Rey & W. R. Buck (2013) Continental and oceanic core complexes. *Bulletin,* 125**,** 273-298.

Yamato, P., L. Husson, T. W. Becker & K. Pedoja (2013) Passive margins getting squeezed in the mantle convection vice. *Tectonics,* 32**,** 1559--1570.

Zhu, G., T. V. Gerya, T. V. Gerya, D. A. Yuen, S. Honda, T. Yoshida & J. A. D. Connolly (2009) Three-dimensional dynamics of hydrous thermal-chemical plumes in oceanic subduction zones. *Geochemistry Geophysics Geosystems,* 10.

Ziegler, P. A. & S. Cloetingh (2004) Dynamic processes controlling evolution of rifted basins. *Earth-Science Reviews***,** 1-50.

Zoback, M. D., R. Apel, J. Baumgartner, M. Brudy, R. Emmermann, B. Engeser, K. Fuchs, W. Kessels, H. Rischmüller & F. a. o. Rummel (1993) Upper-crustal strength inferred from stress measurements to 6 km depth in the KTB borehole. *Nature***,** 633.